

Samson Bergesen

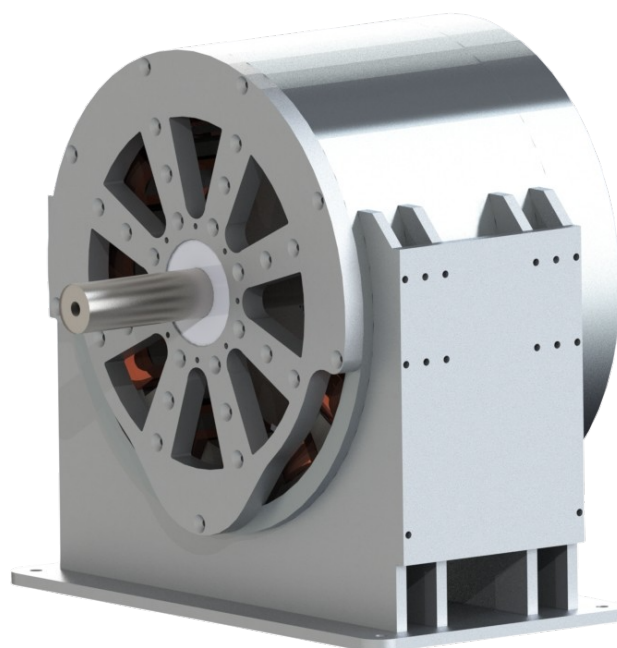
# Design and Manufacturing of a Twin Harmonic Machine with Counter-rotating Rotors

Master's thesis in Energy and Environmental Engineering

Supervisor: Robert Nilssen

Co-supervisor: Arne Nysveen

June 2022



SOLIDWORKS rendering



Samson Bergesen

# **Design and Manufacturing of a Twin Harmonic Machine with Counter-rotating Rotors**

Master's thesis in Energy and Environmental Engineering  
Supervisor: Robert Nilssen  
Co-supervisor: Arne Nysveen  
June 2022

Norwegian University of Science and Technology  
Faculty of Information Technology and Electrical Engineering  
Department of Electric Power Engineering



# Design and Manufacturing of a Twin Harmonic Machine with Counter-rotating Rotors

Samson Bergesen

*Department of Electrical Engineering*

*Norwegian University of Science and Technology*

Trondheim, Norway

June 19, 2022

**Abstract**—The concept of driving two rotors that can rotate in separate directions within the same stator by utilizing harmonic components of concentrated winding layout in a surface-mounted permanent magnet motor has been investigated. The configuration of a number of slots and poles for such a motor was examined, and a stator with 24 slots and two rotors with 22 and 26 poles was chosen. A harmonic analysis was done on this configuration, and it was concluded that it should be able to drive a counter-rotation. The parameters for a motor design with the chosen slot and pole configuration were first analytically done. Then the parameters were simulated using the FEM program COMSOL. COMSOL also confirmed the counter-rotation. Using the motor parameters, a prototype was designed using SOLIDWORKS. The designed prototype was then produced and tested. Finally, a function test performed on the prototype confirmed that the twin harmonic motor drive is possible.

**Index Terms**—Magnetic field harmonics, counter rotation, prototype, hydropower, machine design, harmonic analysis, PM machine, manufacturing

## I. INTRODUCTION

### A. In relations to the specialisation project

During the fall of 2021, the author wrote a specialization project titled "Design of a counter-rotating twin-rotor machine prototype" [1]. Much of the groundwork for this thesis is done in the specialization project, where initial simulations and prototype design were made. The background and the theory behind this thesis and the specialization project are the same, and material from these parts of the specialization project has therefore been reused in this thesis. Some of the results from the specialization project are also presented in this thesis as they are important for the understanding of the work done in the thesis.

The following sections contain parts of reused material from the specialization project and will not be referenced later in the thesis:

- Background and motivation in section I-B
- Theory regarding permanent magnet motors, magnetic field harmonics and cogging factor in section II
- Design process in section III

### B. Background

The capacity of installed renewable energy sources such as wind- and solar power is increasing globally, and these sources are highly uncontrollable with fluctuation in available energy.

The solution for these fluctuations in available energy is power electronics and energy storage [2]. One of the most important energy storage technologies is pumped storage hydropower (PSH), which accounts for 94% of all installed electrical energy storage in the world [3]. PSH has many benefits over other energy storage systems such as battery and flywheel storage systems. PSH allows for energy storage over extended periods of time, a large storage capacity and no use of limited rare earth materials.

Norway relies heavily on hydropower to power its electrical demand, and the total installed capacity in Norway is 33 GW per 2021 [4]. It accounts for 50% of the capacity for hydropower in Europe [5]. The installed PSH is per 2019 at a capacity of 1.4 GW [3] which is around 5% of the total installed capacity in Norway. However, it is estimated that there are 86 hydropower plants with a combined capacity of 10.8 GW that are well suited to be built into PSH [5] [6]. Converting these hydropower plants into a PSH will lead to high cavitation on the turbines as the pressure in the tailrace will be too low in pump mode [5]. The diameter of the installed turbine would also have to be increased to overcome the losses in the waterway [7]. The cavitation wear and the change in waterway and turbine will lead to high costs during the conversion to PSH.

HydroCen is a research center at NTNU that focuses on hydropower technology. HydroCen is currently looking at booster pump solutions to overcome the cavitation problem during pump mode of the hydropower plants. The booster pump solution involves having a booster pump in the tailrace tube to increase the pressure on the suction side of the main turbine, therefore negating the cavitation and waterway losses. This is a considerable cost-saving measure in converting hydropower plants to PSH and could change the conversion from a bad investment to a good one [5]. In the research towards this solution, the booster pump is being designed. Counter-rotating turbines and propellers are considered as they have a hydrodynamic advantage of being able to recover some of the rotational slipstream energy [8]. This would be beneficial for a booster pump for a PSH as the pump would have lower water spin coming up to the main turbine than a conventional single screw turbine. Less water spin would lead to less cavitation and higher efficiency of the main turbine.

The background for this project is based on a phenomenon

that Prof. Robert Nilssen has observed in his many years of working with fractional slot concentrated wound motors which will be described as twin harmonics in this project. The twin harmonics are two harmonics in the magnetic field with different pole numbers and opposite rotations. The twin harmonics often have a much larger magnitude than the other harmonics, sometimes almost as large as the fundamental. Using two rotors with the same number of poles as the two twin harmonics will lead to the rotors having the rotational direction as their respective harmonic. The twin harmonic phenomenon has been investigated in Ole Erik Leangen's master thesis *Achieving counter-rotation by utilizing harmonic components of the magnetic field in a fractional slot concentrated winding permanent magnet motor* [9]. Leangen's thesis concluded that it was possible to drive two counter-rotating rotors in one stator using the twin harmonics but should be investigated further. This project aims to continue the investigation of such a counter-rotating machine.

### C. Scope

This thesis aims to simulate, design, build and test a prototype motor with two counter-rotating rotors, where the counter-rotation will be achieved by using the twin harmonics in the stator. The design for the prototype made in the specialization project "Design of a counter-rotating twin-rotor machine prototype" [1] will be used as the basis for the finished design. Drawings for further improvements and additions to the motor setup will be made using SOLIDWORKS. COMSOL models previously made during the project will also be improved and used to give motor characteristics that will be used during lab testing of the finished prototype. The report will neither include different types of losses nor discuss the general efficiency of the designed prototype as the main goal is to end up with a finished prototype that proves the concept of counter-rotation using magnetic field harmonics. The motor design will not be optimized. Programs such as COMSOL, SOLIDWORKS and MATLAB will be used to simplify the design and simulation process.

### D. Outline

The number of slots and poles will be discussed and investigated, and a configuration is then put into a Matlab script for harmonic analysis. After validating the choice of the number of slots and poles for the motor, the winding layout is presented. Then the preliminary motor parameters are calculated. The parameters are then taken into COMSOL for modelling and verification. Later the final design is made in the CAD program SOLIDWORKS, and the design choices based on manufacturing are disclosed. The manufacturing process and the design changes made along the way are described. Finally, simulation results together with various test results are presented and discussed.

## II. THEORY

### A. Permanent magnet motor

An electric motor is a machine that converts electrical energy to rotational kinetic energy. A permanent magnet

electric motor is a type of electric motor which uses permanent magnets instead of field windings for magnetization. As a result, permanent magnet motors often have high efficiency because they do not have current losses in the rotor windings. Furthermore, as permanent magnet machines are synchronous machines, permanent magnet motors are often talked about as permanent magnet synchronous motors (PMSM). The relation between the rotational frequency of the EMF in hertz ( $f_{el}$ ), and the rotational speed in rpm ( $n$ ), is given by the pole pairs in the machine ( $p$ ) as shown in Equation 1 [10].

$$n = \frac{60 \cdot f_{el}}{p} \quad (1)$$

PMSMs are highly scalable like other electrical machines, where the torque-volume ratio is usually linear. The equation for the rated torque for a sinusoidally-fed PMSM is shown in Equation 2 [11]. The torque can here be computed using the peak value of the fundamental distribution of the flux density in the airgap ( $B_{g1}$ ), linear current density factor ( $K_s$ ), airgap diameter ( $D_{ag}$ ) and the active length of the machine ( $L_{core}$ ). The airgap diameter is defined as the diameter out to the middle of the airgap.

$$T_r = \frac{\sqrt{2}\pi}{4} \cdot B_{g1} \cdot K_s \cdot D_{ag}^2 \cdot L_{core} \quad (2)$$

From this equation, it is possible to see that the rated torque increases linearly with the length of the machine and quadratically with the diameter.

The voltage in a coil is calculated using Equation 3 [12]. By multiplying with the number of coils per phase then this equation can be used to calculate the voltage per phase in an electrical machine.

$$E_{RMS} = \sqrt{2}\pi \cdot k_w \cdot f_{el} \cdot N \cdot \Phi \quad (3)$$

Here  $k_w$  is the winding factor,  $N$  is the number of turns and  $\Phi$  is the total flux per pole. The total flux per pole can be found using Equation 4.

$$\Phi = \frac{2}{p} \cdot B_{g1} \cdot l \cdot r \quad (4)$$

### B. Magnetic field harmonics

A periodic signal can be split into harmonics. Usually, the most dominant harmonic is called the fundamental or first harmonic. A harmonic has a frequency which is an integer multiple of the first harmonic [13]. In electric machines, magnetic field harmonics are a phenomenon created in the stator by the windings. Magnetic field harmonics is a phenomenon that often leads to losses and vibrations.

Figure 1 displays how distributed windings with a phase belt can generate a near perfect sinusoidal magnetic field in the stator. The figure shows one phase of a two-layer winding in which the concentrated coil of  $N_t$  turns has been distributed into four coils per pole, each having a full pitch. In PM motors with high q-factors (number of slots per phase per pole) the MMF tends to be close to sinusoidal, giving low amounts

of harmonic content. PM motors with concentrated windings however, have a lower  $q$  value than motors with distributed windings, giving them a higher amount of harmonic content [14].

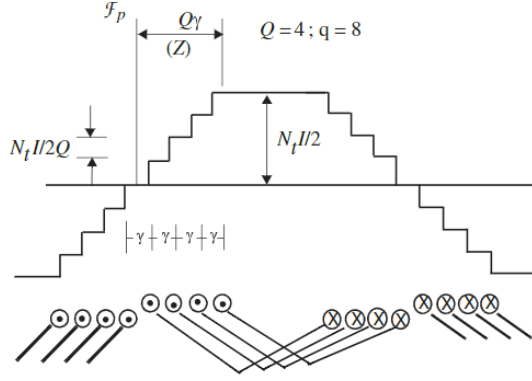


Fig. 1. MMF of distributed winding having four coils in a phase belt [15]

Figure 2 is also a figure from [15]. This figure displays the relative magnitudes of the harmonic components of MMF as determined by the pitch-factor  $k_{ph}$ . As this states, by changing the pitch-factor, one can change the magnitude of different harmonic orders by changing the coil pitch. In ordinary electrical motors, the aim is to reduce any other orders of harmonics than the first one using the pitch factor.

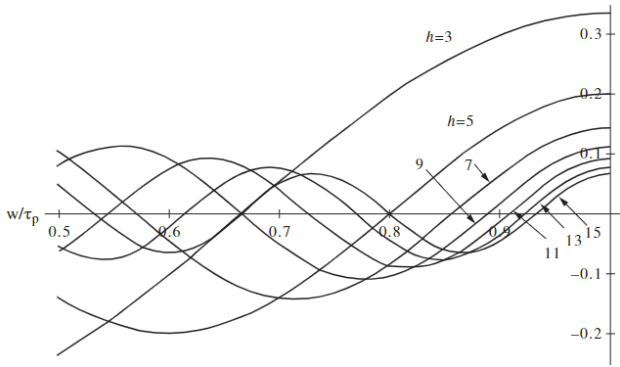


Fig. 2. Pitch factor for harmonics  $h=3, 5, 7, \dots, 15$  as a function of per unit coil pitch  $w/\tau_p$  [15].

The winding produces harmonics with the order  $h$  as shown in 5. Here  $c$  is a factor with the value  $0, 1, 2, 3, 4, \dots$  and  $m$  is the number of phases [16].

$$h = +1 \pm 2cm \quad (5)$$

From this equation, it is possible to see that a symmetrical three-phase winding will have a positive and a negative sequence in the harmonic orders. The negative sequence in the harmonic order will move in the opposite direction. For

example, for a three-phase machine,  $m = 3$ , and a  $c = 3$ , we have two harmonics, one with 11 pole pairs and one with 13 that will rotate in opposite directions.

When the stator is fed with an angular frequency  $\omega_s$ , the angular speed of the harmonic  $h$  with respect to the stator is shown in Equation 6. The harmonic  $h$  will also have pole pairs  $p_h$  referenced to the main harmonic's poles  $p$  as shown in Equation 7

$$\omega_{h,s} = \frac{\omega_s}{h} \quad (6)$$

$$p_h = h \cdot p \quad (7)$$

### C. Cogging factor

The interaction between the MMF harmonics generated by the permanent magnets and the airgap permeance harmonics due to slotting results in cogging torque in PM machines and magnetic gears. This cogging torque manifests as a pulsating torque as the rotor tries to align itself in stable positions. As cogging torque leads to vibrations, it is desired to reduce it as much as possible. The cogging factor ( $f_c$ ) is often used when describing magnetic gears and describes the severity of the cogging torque generated. As stated in [17], the amplitude of the cogging torque is not formally connected to  $f_c$ , but it is proven that a higher  $f_c$  will lead to a higher cogging torque. The formula for  $f_c$  is shown in Equation 8, where  $N_s$  is the number of slots,  $2p$  is the number of poles, and LCM is the lowest common multiple.

$$f_c = \frac{2p \cdot N_s}{\text{LCM}(2p, N_s)} \quad (8)$$

By investigating Equation 8 it can be found that fractional ratios between stator slots and the number of pole pairs result in the lowest cogging factors, this is also explained in [18] and [19].

## III. DESIGN

The design process starts with selecting a stator and rotor configuration that can be used to prove the twin harmonic motor drive concept. Then the parameters for the motor need to be calculated before building a COMSOL model to simulate the design's functionality. After performing the analysis of the functionality of the prototype, the drawings of the motor can be made in SOLIDWORKS.

### A. Selection of number of poles and slots

The first step of the design process was to select the number of slots in the stator ( $N_s$ ) and the number of poles ( $2p$ ) for the two rotors. It is desired that the gearing ratio ( $G_r$ ) between the two rotors is as small as possible so that the deviation in speed and torque between the rotors becomes as small as possible. The gearing ratio is defined as in [18] by Equation 9.

$$G_r = \frac{p_l}{p_h} \quad (9)$$

$p_l$  is the number of pole pairs for the low-speed rotor and  $p_h$  for the high-speed rotor. A configuration with a high number

of slots and a small deviation between the number of poles for the two rotors is favourable. However, a higher number of slots may lead to a lower fill factor and lower structural integrity in the stator teeth. For the prototype to function as optimal as possible, the cogging torque is desired to be as small as possible. Therefore the cogging factor for the different possible configurations of the number of slots and poles has to be investigated. Additionally, in order to have concentrated windings, the number of slots in the stator needs to be a multiple of six. Table I displays the results from the investigation.

TABLE I  
DIFFERENT CONFIGURATIONS OF NUMBER OF SLOTS AND NUMBER OF POLES

| 2p rotor 1 | Number of slots ( $N_s$ ) | 2p rotor 2 | Cogging factor ( $f_c$ ) | Gear ratio ( $G_r$ ) |
|------------|---------------------------|------------|--------------------------|----------------------|
| 10         | 12                        | 14         | 2                        | 0.71                 |
| 14         | 18                        | 22         | 2                        | 0.64                 |
| 16         | 18                        | 20         | 2                        | 0.80                 |
| 22         | 24                        | 26         | 2                        | 0.85                 |
| 20         | 24                        | 28         | 4                        | 0.71                 |
| 26         | 30                        | 34         | 2                        | 0.76                 |
| 28         | 30                        | 32         | 2                        | 0.88                 |
| 34         | 36                        | 38         | 2                        | 0.89                 |
| 32         | 36                        | 40         | 4                        | 0.80                 |

The 24-slot design with 22 and 26 poles for the rotors was chosen for the motor as it has a low cogging factor, a good gear ratio, and does not have too many slots, making this configuration a safe choice. The  $q$  are  $4/11$  for the 22-pole rotor and  $4/13$  for the 26-pole rotor which should, according to theory, give large harmonic content.

### B. MMF harmonic analysis and winding layout

Verifying the number of poles and slot configuration is done by putting the configuration in Prof. Robert Nilssen's MATLAB script for harmonic analysis. When using the harmonics analysis function, the program gives the results shown in Figure 3. From the table in the figure, it is clear that the configuration would provide a high magnitude for the harmonics with 11 and 13 pole pairs, which is promising for the design. This can be explained by looking at Equation 5. Furthermore, it also shows that the configuration for 24 slots with 20 and 28 poles would not have worked as the harmonics with those number of poles are cancelled out.

Using the stator animation tool from the script, the direction of the twin harmonics can be investigated. The harmonic content can be plotted where the 22-pole harmonic is defined as a sub-harmonic and the 26-pole harmonic as a higher harmonic. Figure 4 shows the twin harmonics in the two plots moving in the opposite direction, as required for the motor to work.

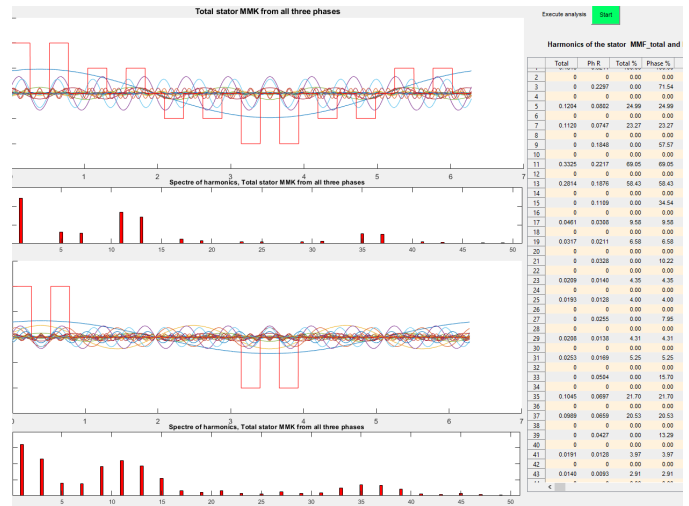


Fig. 3. Harmonic analysis from Matlab program

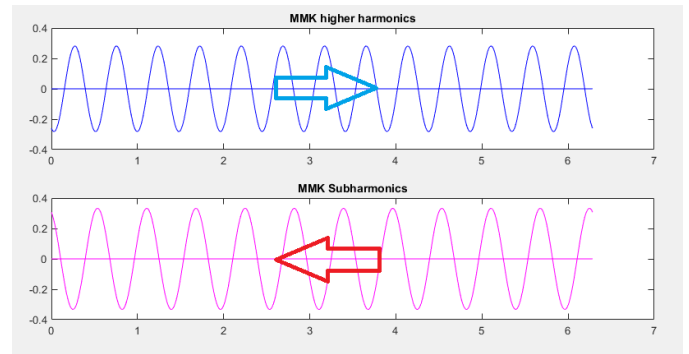


Fig. 4. The two harmonic waves moving in opposite direction

The winding layout for the chosen configuration of 24 slots with concentrated windings was made by using the MATLAB script. The winding diagram can be seen in Figure 5.

| Slot #  | 1  | 2  | 3 | 4  | 5  | 6  | 7  | 8  | 9  | 10 | 11 | 12 | 13 | 14 | 15 | 16 | 17 | 18 | 19 | 20 | 21 | 22 | 23 | 24 |   |
|---------|----|----|---|----|----|----|----|----|----|----|----|----|----|----|----|----|----|----|----|----|----|----|----|----|---|
| Phase R | R  | -R | R | -R |    |    |    |    |    |    |    |    | -R | R  | -R | R  |    |    |    |    |    |    |    |    |   |
| Phase S |    |    |   |    |    |    |    |    | S  | -S | S  | -S |    |    |    |    |    |    |    |    | -S | S  | -S | S  |   |
| Phase T |    |    |   | -T | T  | -T | T  |    |    |    |    |    |    |    |    |    | T  | T  | -T |    |    |    |    |    |   |
| RST     | R  | -R | R | -R | -T | T  | -T | T  | S  | -S | S  | -S | -R | R  | -R | R  | R  | T  | -T | T  | -T | -S | S  | -S | S |
| Bottom  | -S | -R | R | -R | R  | T  | -T | -T | -S | S  | -S | S  | R  | -R | R  | -R | -T | -T | T  | -T | T  | S  | -S | S  |   |
| SingleP | R  | -R | R | -R |    |    |    |    |    |    |    |    | -R | R  | -R | R  |    |    |    |    |    |    |    |    |   |
|         |    |    |   |    |    |    |    |    | S  | -S | S  | -S |    |    |    |    |    |    |    |    | -S | S  | -S | S  |   |
|         |    |    |   |    |    |    |    |    | -T | T  | -T | T  |    |    |    |    |    |    |    |    | T  | -T | T  | -T |   |

Fig. 5. Winding layout

### C. Initial specifications

Since the purpose of the prototype motor is to prove the concept of driving a motor using the twin harmonics, there were no initial set performance specifications, and the motor will therefore not be optimized. However, a starting point for the design process is needed, and the rated power is set to

2 kW (1 kW per rotor) with an outer diameter required to be 300-400 mm. The power requirement is set since motor controllers of this size are easily obtainable, and the size requirement is set for the motor to be relatively easy to move around. To ease the assembly of the prototype and hopefully increase the twin harmonic phenomenon, the motor will be designed with concentrated windings. Having concentrated windings will also allow for higher magnitudes of the higher harmonics. As it is easiest to test the prototype in a low voltage lab, the prototype will be designed for being operated with a phase voltage of 230 V, resulting in a desired rated current of 2.9 A. The electrical frequency is also assumed to be 50 Hz. However, this can be changed during testing to check the speed characteristic of the motor. The two rotors are expected to act as two motors in series, resulting in 115 V per phase. With the power rating and the electrical frequency, the speed and torque for each rotor are also set. The rotational speed for the 22-pole rotor will be 272.7 RPM with a 35 Nm torque, while the speed of the 26-pole rotor is 230.8 RPM with a torque of 41 Nm.

#### D. Initial calculations

The first analytical dimensioning was done using the procedure described in the *Sizing procedure of surface-mounted PM machines for fast analytical evaluations* paper [11]. In short, this procedure bases itself on designing the stator iron based on the preliminary set requirements for the max flux density in the stator teeth ( $B_{ts-max}$ ), stator yoke ( $B_{ys-max}$ ), rotor yoke ( $B_{rs-max}$ ) and the max current density ( $J_{max}$ ). The stator teeth width ( $w_{tt}$ ) and stator yoke height ( $h_{ys}$ ) are dimensioned to account for the max stator teeth and yoke flux density respectively, using Equation 10 and 11. The flux density is calculated from the size and strength of the magnets. The stator teeth height is then dimensioned to give a slot area that can account for the set slot current density, using Equation 12. The motor is designed with straight slots to ease the windings' fitting during the prototype's assembly. The rotor yoke thickness can be dimensioned, iterating around the flux density in the rotor. However, as the inertia is not considered a problem and the cost of the rotors would be unchanged, the rotors are designed as solid discs with the inner radius equal to the outer radius of the shaft.

$$w_{tt} = \frac{B_g}{B_{ts-max} \cdot K_i} \cdot (\alpha_m \cdot \tau_p - \frac{\tau_s - \tau_p}{2}) \quad (10)$$

$$h_{ys} = \frac{B_g \cdot \alpha_m \cdot \tau_p}{B_{ys-max} \cdot K_i \cdot 2} \quad (11)$$

$$h_{us} = \frac{K_s \cdot \pi \cdot D_{is}}{J_{max} \cdot N_s \cdot k_{wdg} \cdot k_{fill} \cdot w_{tt}} \quad (12)$$

Here  $B_g$  is the maximum flux density in the airgap,  $K_i$  is the lamination pack coefficient,  $k_{wdg}$  is the winding factor,  $k_{fill}$  is the fill factor,  $D_{is}$  is the inner stator diameter,  $\tau_p$  is the polar pitch,  $\tau_s$  is the stator slot pitch and  $\alpha_m$  is magnet width as a percentage of the pole pitch. The linear current density factor

was calculated using Equation 2 using the desired torque as input.

The slot pitch and pole pitch are defined by Equation 13 and 14.

$$\tau_s = \frac{\pi \cdot D_{is}}{N_s} \quad (13)$$

$$\tau_p = \frac{\pi \cdot (D_{is} - 2 \cdot h_{ag} - l_m)}{2 \cdot p} \quad (14)$$

The initial specifications for the motor were set to relatively moderate values. As the materials to be used in the prototype were not chosen at the beginning of the design process, the moderate values would prevent any saturation or overheating. However, selecting moderate values could also lead to the motor being somewhat over-dimensioned. The initial specifications are shown in Table II.

TABLE II  
INITIAL SPECIFICATIONS

| Parameter                 | Symbol   | Unit              | Value |
|---------------------------|----------|-------------------|-------|
| Stator yoke flux density  | $B_{ys}$ | T                 | 1     |
| Rotor yoke flux density   | $B_{rs}$ | T                 | 1     |
| Stator tooth flux density | $B_{ts}$ | T                 | 1     |
| Slot current density      | J        | A/mm <sup>2</sup> | 2     |

The starting dimension for the calculation process was the inner stator diameter and the length of each rotor. The inner stator diameter was set to 270 mm as this would lead to an outer diameter of around 300-400 mm as initially specified, while the length of each rotor was set to 40 mm. Rotor lengths were selected as the magnet length of 40 mm was readily available. The magnet's dimensions were set so that the magnets would not be too strong, making the manufacturing process harder and making the magnets more costly. The magnet vendor called *supermagnete* was used to find suitable magnets for the project [20]. The magnet dimensions were set to be 40 X 20 X 5 mm. The magnets would then cover the entire length of the rotors while not being too wide to fit on the 26-pole rotor.

Using Equation 3 the number of turns can be calculated where the desired voltage per phase is set to 230 for the two rotors in total. Emeter's winding factor calculator [21] is used to find the winding factor, and it calculates that the winding factor for the two rotors is 0.955. Assuming a peak flux density between 0.9 and 1 in the airgap, the required number of turns is found to be 150. The most available wire thickness in the workshop was 1.3 mm<sup>2</sup>, which could hold up to 3.7 A RMS continuously according to the American Wire Gauge Chart (AWG chart). Using this copper wire with 150 turns and the set slot area of 308 mm<sup>2</sup> would require achieving a fill factor of 63%.

After finishing the dimensioning process, the final motor parameters is shown in Table III. These parameters were taken onwards to the Finite Element Analysis (FEA) models of the motor.

TABLE III  
PROTOTYPE CALCULATED DIMENSIONS

| Parameter             | Symbol       | Value [mm] |
|-----------------------|--------------|------------|
| Outer rotor diameter  | $D_{er}$     | 258        |
| Outer stator diameter | $D_{es}$     | 350        |
| Inner stator diameter | $D_{is}$     | 270        |
| Inner rotor diameter  | $D_{ir}$     | 40         |
| Airgap height         | $h_{ag}$     | 1          |
| Useful slot height    | $h_{us}$     | 26         |
| Stator yoke height    | $h_{ys}$     | 14         |
| Length per rotor      | $L_{rotor}$  | 40         |
| Length stator         | $L_{stator}$ | 150        |
| Magnet width          | $w_m$        | 20         |
| Slot width            | $w_{st}$     | 16         |
| Stator tooth width    | $w_{tt}$     | 19.3       |

### E. FEM analysis

To verify the design of the prototype, two cross-sections models were built in COMSOL, one for each rotor. The models were made to analyse and verify the counter-rotation of the motor. Each model includes one of the rotors, where the interaction between the rotor and stator can be investigated. As the rotors only can be analysed separately, the interaction between the rotors, such as cogging between the rotors, can not be investigated. The model with the 26-pole rotor can be seen in Figure 6. In the model, four layers were added to the airgap to make the mesh in the airgap symmetrical.

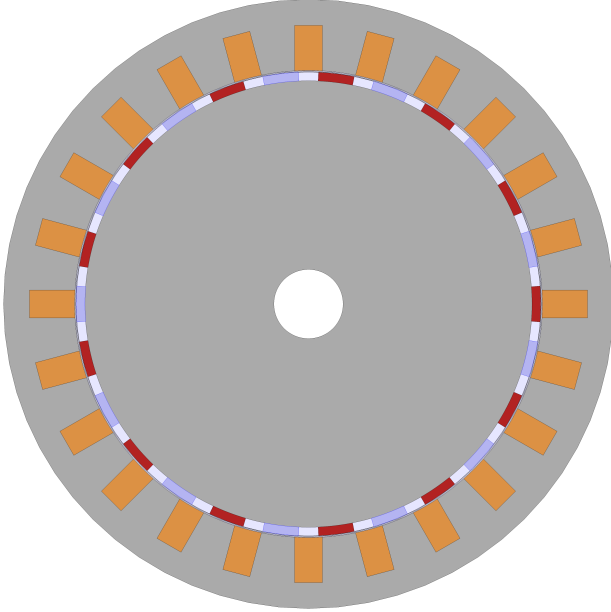


Fig. 6. Geometry of the model with 26 poles

Under physics, two amperes laws were added to separately define the radially north and south-facing magnets. On Figure 6 the north and south pole of the magnets can be seen as blue and red, respectively. An amperes law was also added to define the magnetic flux saturation curve for the rotor and

stator iron. The saturation curve was set to the predefined BH-curve given by COMSOL. This BH-curve is set to saturate at around 1.5 T, which was considered reasonable. Three coil physics were added to define the phases in the stator and assigned according to the winding layout seen in Figure 5. The currents added can be seen in Table IV. Finally, a force calculation was added to the rotor and the inner layer of the airgap.

TABLE IV  
PHASE CURRENTS

| Phase | No load | On load                                    |
|-------|---------|--|
| A     | 0       | $\hat{I} \cdot \sin(2\pi f_{el})$          |
| B     | 0       | $\hat{I} \cdot \sin(2\pi f_{el} + 2\pi/3)$ |
| C     | 0       | $\hat{I} \cdot \sin(2\pi f_{el} + 4\pi/3)$ |

For accurate results, the meshing of the model is essential. The airgap flux determines the motor's torque, and this mesh is therefore emphasized in the model. As pointed out earlier, the models were made with four layers in the airgap to ensure a symmetrical and high quality mesh in this area. The meshing in the stator and rotor iron is less crucial and therefore requires lower meshing to reduce the simulation time. The meshing difference between the airgap and the rest of the model can be seen in Figure 7.

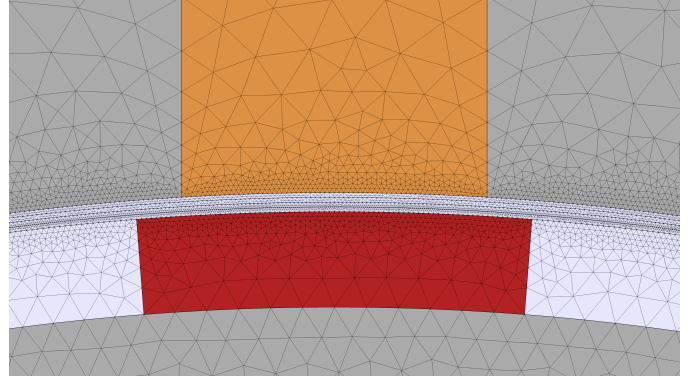


Fig. 7. Mesh of the model near the airgap

A locked rotor test was done where the currents were set according to Table IV, and the rotational speed was set to zero. The locked rotor test was done to find the  $\delta_q$ , which is the angle displacement applied to the current to align the current with the q-axis of the motor, also called time shift. The simulations were run for one electrical rotation  $T_{el}$  with 200 steps. The locked rotor test gave the curve shown in Figure 8 for the 26-pole rotor and a similar one for the 22-pole rotor. The two rotors needed two separate time shifts as they rotate in opposite directions, and what is considered max torque has opposite signs. The time shifts are found using the COMSOL functions 'attimemax' and 'attimemin'. The time shifts are found to be 0.0062 seconds for the 22-pole rotor and 0.0163 seconds for the 26-pole rotor. This resulted in the angles being:  $\delta_{q,22} = t_{max-torque} \cdot f_{el} \cdot 360^\circ = 0.0062 \cdot 50 \cdot 360^\circ = 111.6^\circ$

$$\delta_{q,26} = 0.0163 \cdot 50 \cdot 360^\circ = 293.4^\circ$$

These angles might be a source of error as most motor controllers cannot drive motors at such an optimal angle.

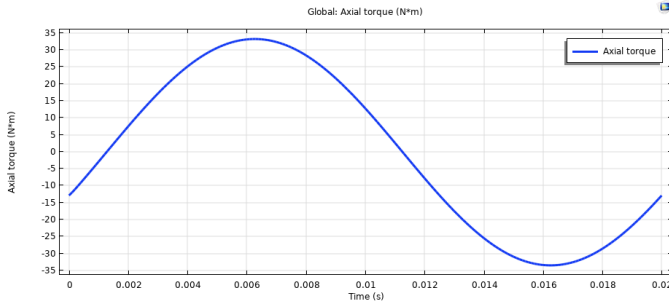


Fig. 8. Locked rotor test

### F. SOLIDWORKS model

The designed motor was drawn and modeled using SOLIDWORKS. A cross-sectional view of the final design setup for the prototype is shown in Figure 9. In the figure copper windings, bearings, and feet for the motor are added and set up for illustrative purposes. With this setup, one rotor shaft will be mounted with ball bearings in the cover of the stator housing, while the other rotor shaft will be mounted on an adjustable table with pillow block bearings. The rotor shaft mounted with pillow block bearings will be movable, allowing the distance between the rotors to be adjusted. Therefore, it is possible to investigate the rotors' influence on each other. The distance between the rotors will be adjusted using a spacer seen to the left in Figure 9. Using a bolt with a known thread pitch, the distance can be adjusted by turning the bolt with the right amount of turns. To have room for the distancing between the rotors, the stator needs to be longer than the combined length of the two rotors. Therefore, the stator length is set to 150 mm, allowing the rotors to be adjusted up to 70 mm apart.

The original stator design was modified to have straight slots, also called parallel slots, as shown in Figure 10. This change will allow the coils to be wound and formed beforehand and then slid onto the straight tooth, significantly simplifying the assembly process of the motor. Changing the design to parallel slots resulted in a smaller slot area, leading to a higher slot current density. However, increasing the slot current density is considered not to be an issue as the motor is a bit over-dimensioned. Marking slots with a radius of 1.5 mm were added along the stator edges. These are used for the alignment of the stator stacks during stator manufacturing. The marking slots are best illustrated in Appendix A. The stator has to be assembled from stacked laminated iron to avoid high current losses in the stator. The laminations can either be laser-cut or stamped out. To stamp out the laminations, the stamping tools have to be made, which is costly for small-scale production, making laser-cutting more viable for this project.

The two rotors are designed to be held on the shafts with a 1 mm tall and 2 mm wide edge on the innermost part of

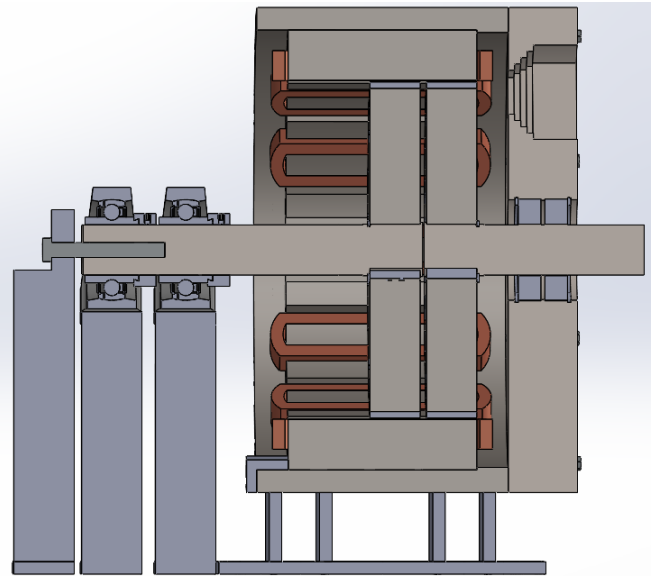


Fig. 9. Cross-section view of the setup for the designed prototype

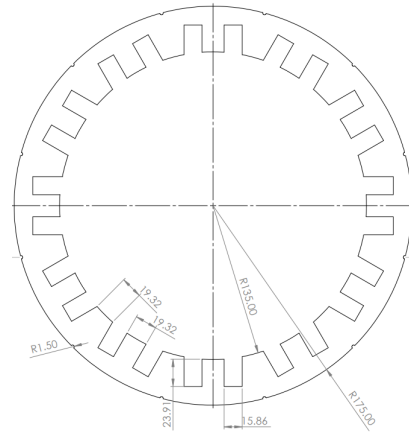


Fig. 10. Final stator design

the shaft and a retaining ring on the other side of the rotor, dimensioned after [22]. With these dimensions for the edge holding the rotors in place, the distance between the rotors can be as small as 5 mm when the distance between the shafts is 1 mm. If the retaining rings were to be set where the edge is, the mounting of the rotors could have been easier, but the smallest distance between the rotors would be 12.3 mm. The smallest possible distance between the rotors for the test setup is desired to test the effect the rotors have on each other thoroughly. The rotors are secured with a wedge, securing that the rotors cant rotate without the shafts. The wedge is also dimensioned according to [22]. To secure the alignment of the rotor magnets, the rotors are designed with magnet beds. Misalignment of the magnet placement can influence the cogging and general function of the motor and is therefore considered crucial during manufacturing. The bed for the magnets need to be cut 2 mm into the rotors to secure that the

magnets can not move, and the rotor diameters are increased by 4 mm to account for the magnet beds. The assembly of the rotors can be seen in Figure 11. The rotors are to be laser-cut from the same laminations as the stator stacks. Having laminated stacks for the rotors is more important for this motor than other motors as the laminations prevent current losses in the rotors. Current losses in the rotor might influence the magnetic field harmonics in the motor, which is crucial for this prototype. All dimensions for the rotors can be seen in Appendix B and C.

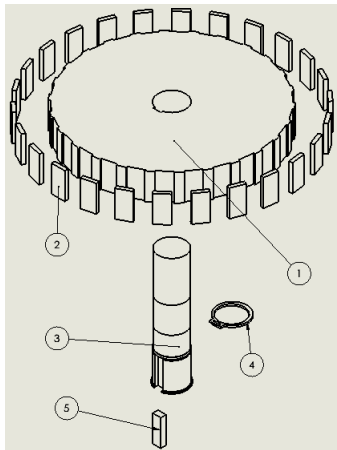


Fig. 11. Assembly of the rotor to the rotor shaft

A stator housing and its cover are also designed to hold everything together. Figure 12 shows the planned assembly for the stator housing. Two bearings (2) are to be fitted in the cover of the stator housing (3) as two bearings are needed for the stability of the shaft. The bearings will be held in the cover with two retaining rings (1). The stator (5) is to be held in the housing (4) using three fasteners (6). The fasteners are to be bolted into the housing, pushing the stator against an edge inside the housing. The cover and stator housing dimensions can be seen in Appendix D and E.

#### IV. MANUFACTURING

The prototype's manufacturing process brought challenges that required clever solutions and design changes. This section will focus on the most important manufacturing steps in the manufacturing process.

##### A. Manufacturing steps

1) *Laser cutting rotors and stator:* The production of the stator and two rotor stacks were outsourced as they needed to be laser cut, which was not possible to do in-house. The stacks were laser cut lamination stacks and bonded by LCD LaserCut AG. Magnetic steel of the type M330-50A was used as this was recommended by the supplier. In Figure 13 the stator and rotor stacks can be seen as they were delivered.

2) *Machining stator housing:* Originally the stator housing and cover were planned to be machined out in the workshop at NTNU. However, it was discovered that the maximum diameter possible to be used in the lathe at NTNU was

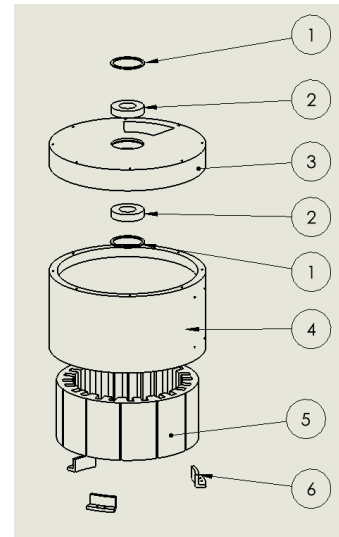


Fig. 12. Assembly of the stator housing



Fig. 13. Laser cut parts

350 mm, and the outer diameter of the stator housing is 386 mm. This restriction meant that the machining of the housing and cover had to be outsourced as well.

Delprodukt AS machined the stator housing and cover from a grade 6082-T6 aluminium bar. The housing and cover can be seen in Figure 14. Later, a window was added to the drawings and machined in the workshop to allow viewing of both rotors during operation.

3) *Building stand for the stator housing:* The stator housing needed a stand, which wasn't designed originally. Using SOLIDWORKS, the stand was designed to be made from aluminium plates, as this would allow them to be water cut at the workshop. Figure 15 displays the finished housing stand design from SOLIDWORKS. All the housing stand drawings can also be seen in Appendix F. One of the sides has a larger plate where the junction box is meant to be mounted. The drawings were exported as DWG files and water cut before they were assembled onto the stator housing.

4) *Fitting stator into the stator housing:* The stator was hammered into the stator housing until it hit the edge designed

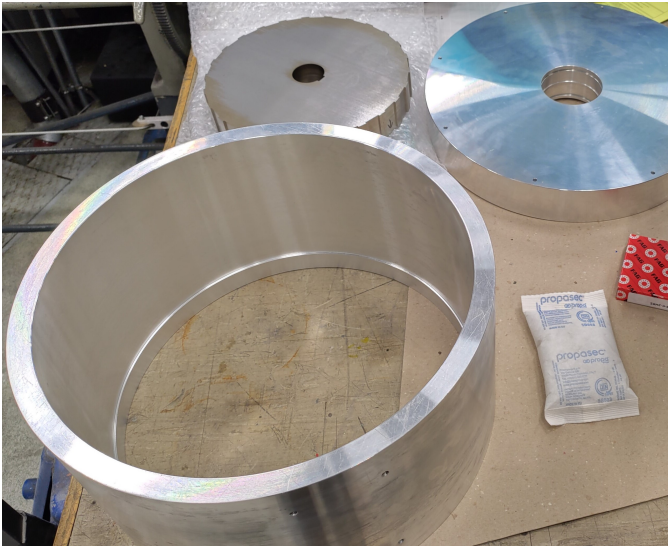


Fig. 14. Stator housing and cover

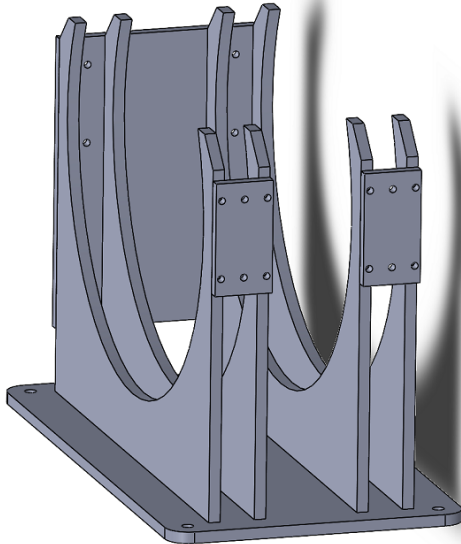


Fig. 15. Housing stand design

to keep it in place. During this process, it became evident that the original solution for keeping the stator in place using a clamp was redundant as the fit of the stator was so tight it would not be able to move with the expected torque that would affect it. The stator in the housing can be seen in Figure 18.

5) *Winding and fitting coils:* During planning for winding of the coils, it was decided to design and 3D print a holder that the coils would be wound around. These holders were only meant to be used during the winding to help shaping the coils, but later during the design process, using the coil forms to hold the coils in place in the stator was decided. Using the holders to hold the coils in the stator would limit the need for glue on the coils, make the fitting of the coils in

the stator easier, and give protection for the coils during the fitting of the coils. The coil forms would also provide some protection during the motor assembly and electrical insulation between the coils and the stator iron. As the holders were to hold the coils in place and keep the coils from moving towards the rotors during operation of the motor, the holders were designed with flanges on top that would hold the coils in the slots. A holder for the coil forms to use during the winding of the coils was also designed and 3D printed. The finished coil form (1) design and the holder (2) for it can be seen in Figure 16. Using red, blue and green PLA, the coil forms were colour coded to represent the phases. The colour coding was done to make the connection of the coils easier and to improve the aesthetic of the prototype when finished.

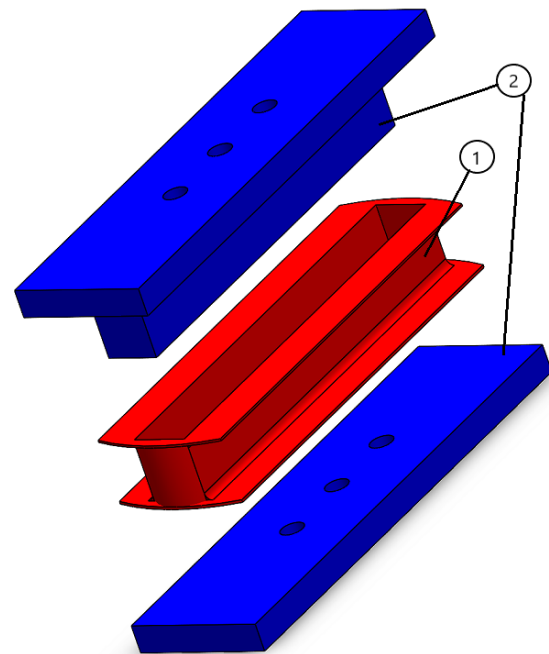


Fig. 16. Coil form with holder used during winding

Winding of the coils was done using a winding machine turned by hand with a counter connected. A plastic sheet was placed in the coil forms to ensure that electrical insulation between the coils and the stator iron was good enough. The plastic sheet was placed with one side between the coil and the coil form and a larger piece hanging out that would wrap around the coil when pushed into the stator. After a coil was wound, electrical tape was wrapped around the coil to ensure that it did not unwind during fitting the coils in the stator. Figure 17 shows the process of winding the coils. One advantage of using coil forms for the winding process was that the coils easily could be test fitted in the stator to check for faults in the design, such as the coil forms fitting as intended or if the number of turns was too high or too low. However, during the test fittings of the coils, it was discovered that they were extruded too much to the sides to fit with the planned 150 turns. The number of turns was therefore changed from 150 to 130, requiring a fill factor of 54% rather than 63%.

The change would lead to the rated phase voltage changing from 230 V to 200 V as well as changing the rated current from 2.9 A to 3.3 A

The first iteration of the coil forms was designed to take as little as possible space away from the coils and had thin walls and only thin flanges on the top to hold the coils in place in the stator. However, during the first fitting of the coils, it was discovered that the holders were soft and prone to cracking. To improve the structural integrity of the holders, flanges were added to the bottom of the holders as well. The coils were grinding towards the sharp stator edges on the bottom of the slots, which was a problem that the bottom flanges of the coil forms also helped to overcome. The winding process had to be repeated multiple times as the pressure that the coils were wound with had to be tuned since the pressure from the coils sometimes broke the coil forms. Here the advantage of 3D printing the forms came into play, as the forms could easily be remade or redesigned. During the iterations of the coil forms, some steps were taken to increase the structural integrity of the forms. In addition to flanges that were added on the bottom of the forms, walls in the coil forms were made thicker and more material to hold the flanges was added.

could be test fitted in the stator to check for faults in the design, such as the coil forms fitting as intended or if the number of turns was too high or too low.

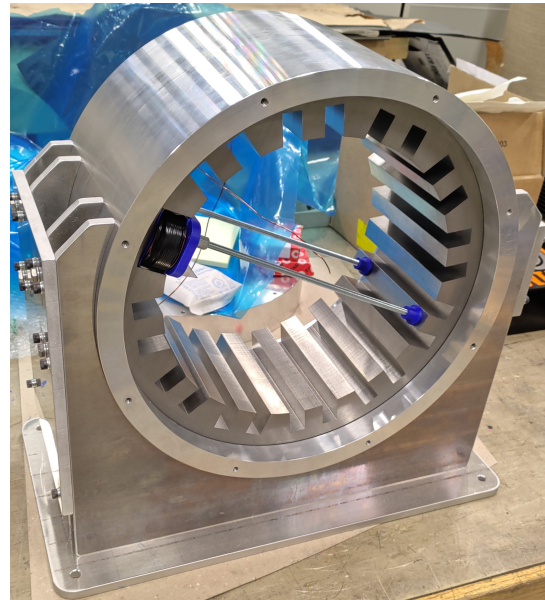


Fig. 18. Gluing of the coils

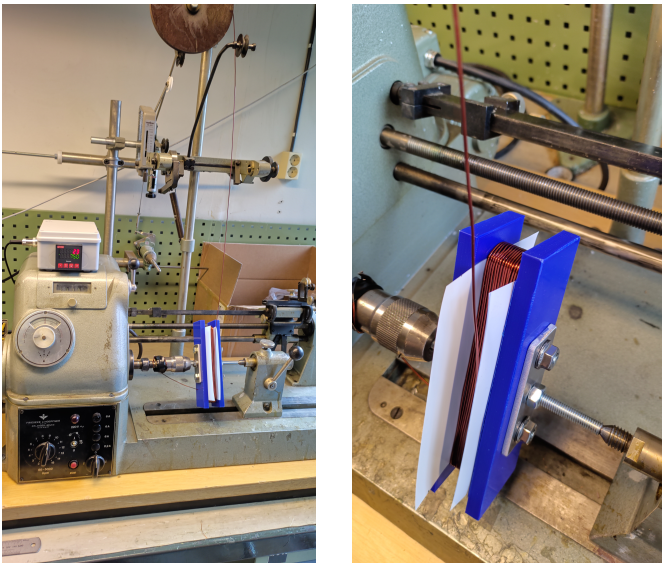


Fig. 17. Winding process of the coils

Winding of the coils was done using a winding machine turned by hand with a counter connected. A plastic sheet was placed in the coil forms to ensure that the electrical insulation between the coils and the stator iron was good enough. The plastic sheet was placed with one side between the coil and the coil form and a larger piece hanging out that would wrap around the coil when pushed into the stator. After a coil was wound, electrical tape was wrapped around it to ensure that it did not unwind while fitting the coils in the stator. Figure 17 shows the process of winding the coils. One advantage of using coil forms for the winding process was that the coils easily



Fig. 19. All coils glued in the stator

6) *Electrical connections:* After the coils had been glued to the stator, the wires from the coils were measured and cut to the correct lengths. The wires were then insulated using the same colour coding as the coil forms and connected using splicing connectors. It was decided to use splicing connectors

instead of soldering the wires to make eventual corrections along the process easier. All the wires were then fastened to the stator housing using plastic strips.

A junction box was mounted on the junction box plate on the motor stand. All the terminals for the phases were guided to the junction box, bundled together in a cable sleeve and connected to banana plug connectors. In addition, a grounding cable connected to the junction box plate was also guided into the junction box and connected to a banana plug connector.

7) *Assembly of the rotors:* The assembly process of the rotors can be seen in Figure 11. The assembly of the rotors started with gluing the magnets (2) into the slots on the rotor stacks. Due to the importance of having the correct polarity in the correct slot, the polarity of the magnets was checked and marked carefully. The magnets were carefully glued into the slots in the rotor, using a Teflon working surface to avoid accidentally gluing parts to the working surface.

The next step in the assembly process of the rotors was to assemble the rotors to the shafts. First, the rotors were slid onto the shafts (3) until they hit the edge of the shaft. Then, retaining rings were placed on the other side of the rotors (4), and wedges were slid into the rotors (5).

8) *Aligning of the rotors:* The alignment of the rotors started with the rotor mounted in the stator housing cover, which was chosen to be the 26-pole rotor. This process can be seen in Figure 20 and 21. Firstly the bearing on the inside of the cover was entered (1) in the cover and secured with a retaining ring (2). Then the shaft of the rotor was entered in the bearing (3) before the other bearing was fitted on the other side of the cover and secured with a retaining ring (4) and (5). The cover with the shaft and rotor was then hoisted up using an eyebolt fastened in the shaft and lowered into the stator (6). A 1 mm thick metal plate was placed on the inside of the stator to help center the rotor. The metal plate was removed from between the rotor and stator when the cover was bolted in place in the stator housing. As the cover and housing were machined with good accuracy, the rotor was perfectly aligned and had next to no cogging torque. Figure 22 displays the motor with one rotor aligned.

The alignment of the the 22-pole rotor started with assembling a small table of aluminium extrusions to mount the pillow block bearings. The steel plate which the pillow block bearings were mounted to was placed on rails to make the adjustment of the rotor distance possible. A long threaded bolt was added to the table and the steel plate to make the rotor distance easier to adjust. Thin metal spacers were added under the pillow block bearings to adjust the height of the rotor, and small bolts were mounted on the sides of them to adjust the sideways alignment. The first attempt at aligning the rotor was made using an Easy-Laser, a tool that uses a laser to determine the offset from one shaft to the other in all directions. This was very difficult as the Easy-Laser is intended to have one common axis through the entire machine, which this prototype doesn't have with its double shaft design. This meant that when the laser was rotated around the axis of one of the shafts, the receiver on the other shaft didn't rotate along

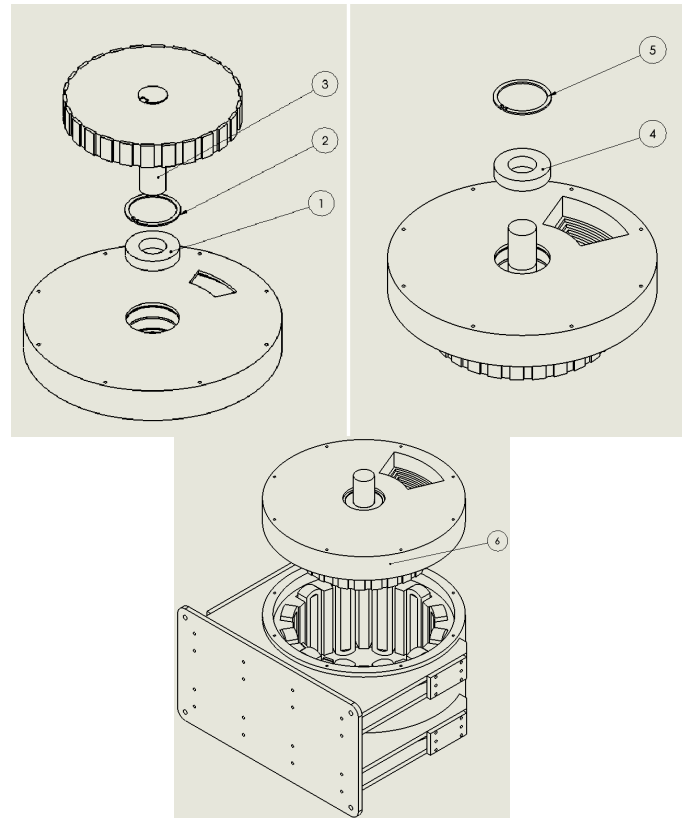


Fig. 20. Assembly of the first rotor

with the laser, making the readings inaccurate.

Therefore the alignment of the rotor had to be done manually using thin 0.5 mm plates of stainless steel to measure the distance between the rotor and the stator on the top, bottom and both sides. After numerous attempts, it was discovered that the magnetic forces from the rotor were strong enough to bend the entire aluminium table, making the alignment impossible. Therefore a new table water cut from steel plates was made. In addition, the bearings were moved closer to the rotor as the bending of the shaft combined with movement in the bearings also made the alignment of the rotor impossible.

After a couple of attempts, the other rotor was then aligned and inserted into the rotor, which can be seen in Figure 24. Unfortunately, the alignment of the second rotor was not as perfect as the first one, which resulted in a more significant cogging torque than anticipated. Moving the bearings closer to the rotor also resulted in the rotor being almost on the edge of the stator, making it impossible to test the influence of the distance between the rotors. To do the rotor distance test, a new sturdier shaft would have to be made, and new pillow block bearings would have to be bought.

A function test was done to both prove that the prototype worked and to determine if the cogging was too severe for further testing to be done further. This is described in subsection V-D. During this testing, it was discovered that the vibration caused by the cogging was too severe for further testing.

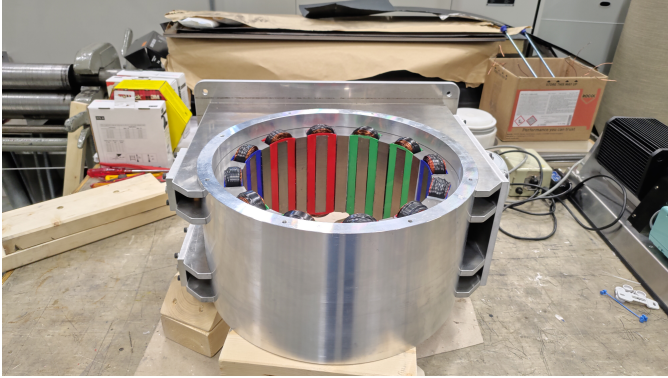
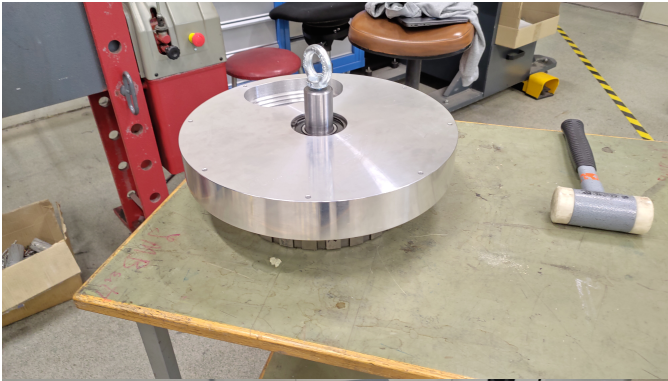


Fig. 21. Entering the first rotor

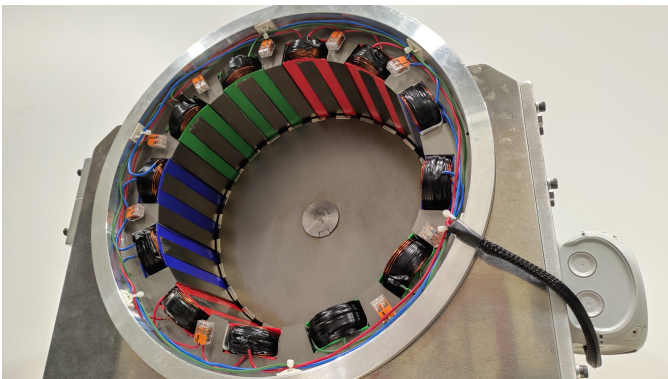


Fig. 22. First rotor fitted

To make the alignment possible, a 60 mm shaft was made for the the 22-pole rotor. The new shaft setup can be seen in Figure 25. New larger pillow block bearings were also bought to fit the new larger shaft. A cover able to hold a bearing was also made for the open side of the stator housing. This cover was created using the in-house water cutter and was made from two plates of aluminium stacked beside each other. The rotor was assembled to the shaft before the shaft was tread into the bearing in the cover and the two pillow block bearings. The pillow block bearings were fastened onto the table again before the the 22-pole rotor once again was inserted into the stator. The new cover created a common centre point through

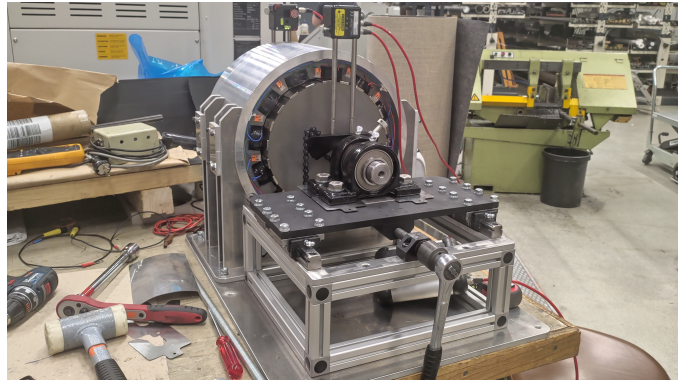


Fig. 23. Alignment of the the 22-pole rotor with aluminium table

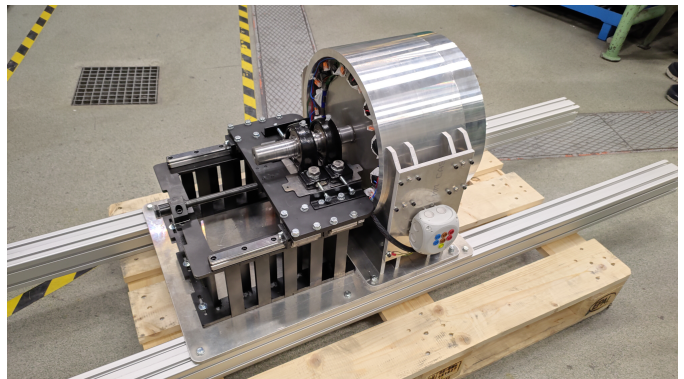


Fig. 24. First attempt at aligning the 22-pole rotor



Fig. 25. New 60 mm shaft setup

the motor, making it possible to use the Easy-Laser to align the rotor. After the alignment process on the the 22-pole rotor was

done, the cogging torque for this rotor also was satisfactory. The finished motor setup can be seen in Figure 26.

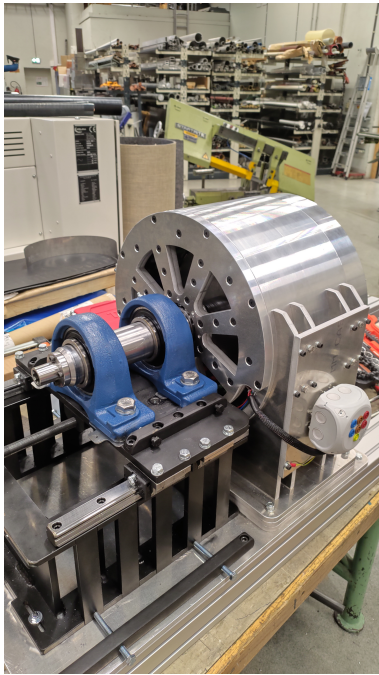


Fig. 26. Finished motor setup

## V. TESTING AND RESULTS

During the project period, simulations and various tests were performed on the designed prototype. This section will focus on the simulations, tests and results from these. The simulation results were used to give expectations for the tests performed on the prototype. Some of the tests performed resulted in design changes.

### A. Simulation results from COMSOL

The COMSOL models made for the verification of the counter-rotation of the two rotors were run with rated values. The current was however set to 3 A instead of 3.35 A as it was considered too close to the current limit of the wire, leaving safety margin. Two main tests were performed in COMSOL. In the first test the rotors were rotated with rated speeds with no current load, here called no-load test. In the second test the current and rotations of the rotors was set to nominal values, here called the nominal test.

1) *No-load operation:* First, the no-load test was performed on the two COMSOL models. The torque results from the no-load test can be seen in Figure 27 and 28. These figures show that the cogging torque is offset, where cogging torque normally oscillates around the 0 Nm line. The reason for the cogging torque being offset in the positive direction for the 22-pole rotor while being offset negative for the 26-pole rotor is likely caused by the opposite rotational direction.

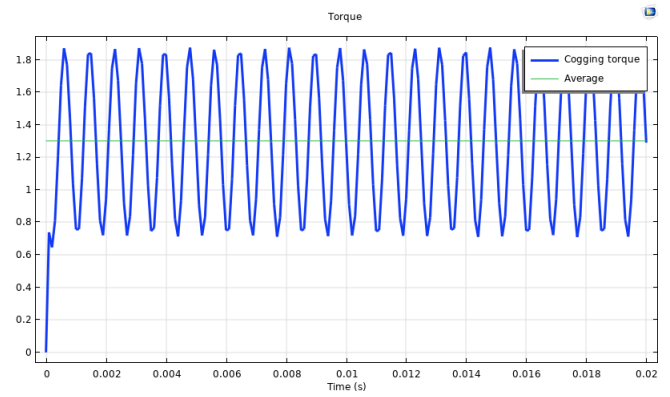


Fig. 27. Cogging torque 22-pole rotor

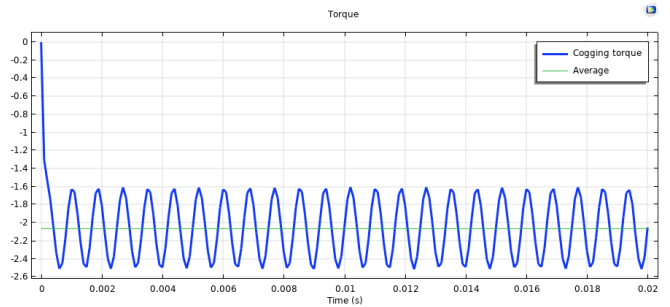


Fig. 28. Cogging torque 26-pole rotor

The back emf for the two rotors is shown in Figure 29 and 30. The two curves show a slight difference in voltage and in voltage shape.

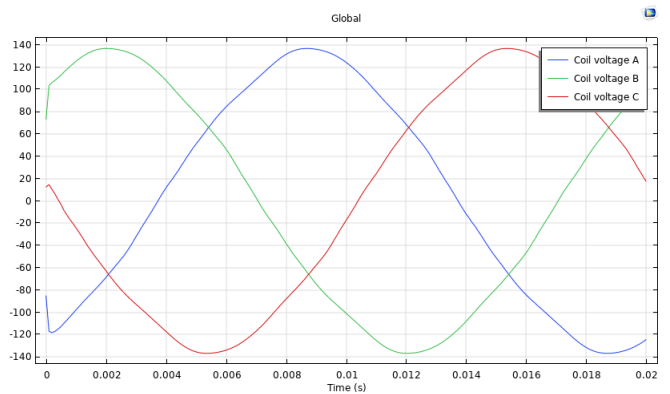


Fig. 29. Back emf on the 22-pole rotor

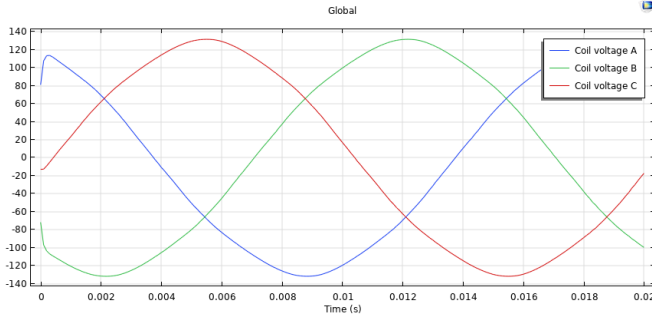


Fig. 30. Back emf on the 26-pole rotor

2) *Nominal test*: The simulation with nominal values is run on the motor. The nominal torque curves can be seen in Figure 31 and 32. The torque has opposite signs for the two rotors when the rotational speed is set to rotate in the opposite direction of each other, proving a counter-rotation.

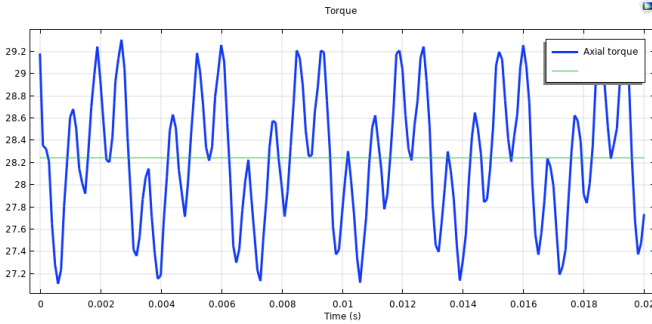


Fig. 31. Nominal torque curve for 22-pole rotor

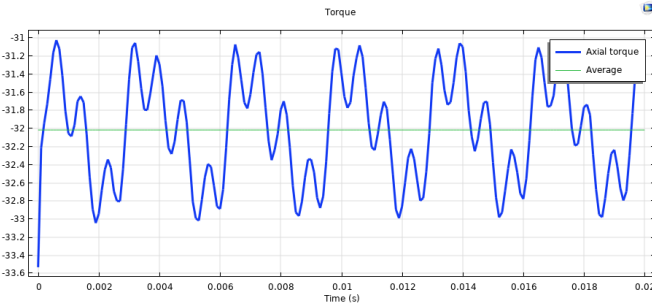


Fig. 32. Nominal torque curve for 26-pole rotor

From the nominal test and the no-load test, the nominal torque, cogging torque and torque ripple were found. The cogging torque can be found looking at the average value from the no-load test from Figure 27 and 28, or by subtracting the maximum torque value from the minimum torque value shown in Figure 31 and 32. The nominal torque is found using average torque value for the curves, and torque ripple is found using Equation 15. For these operations the *timemax*, *timemin*

and *timeavg* functions in COMSOL are used as these functions find the maximum, minimum and average values respectively from a set curve. The results are shown in Table V.

$$T_{ripple-\%} = \frac{T_{max} - T_{min}}{T_{avg}} \cdot 100\% \quad (15)$$

TABLE V  
TORQUE RESULTS

| Rotor Poles | Nominal Torque [Nm] | Cogging Torque [Nm] | Torque Ripple [%] |
|-------------|---------------------|---------------------|-------------------|
| 22          | 28.2                | 2.2                 | 7.7               |
| 26          | 32                  | 2.2                 | 6.1               |

The cogging torque found from the nominal test was higher than expected from the no-load test for the 22-pole rotor. This increase in cogging could come from a magnetic field harmonic interference that does not occur before the current is put on in the stator. The torque ripple is slightly on the high side but is considered acceptable for a prototype that is not supposed to be driven over extended periods.

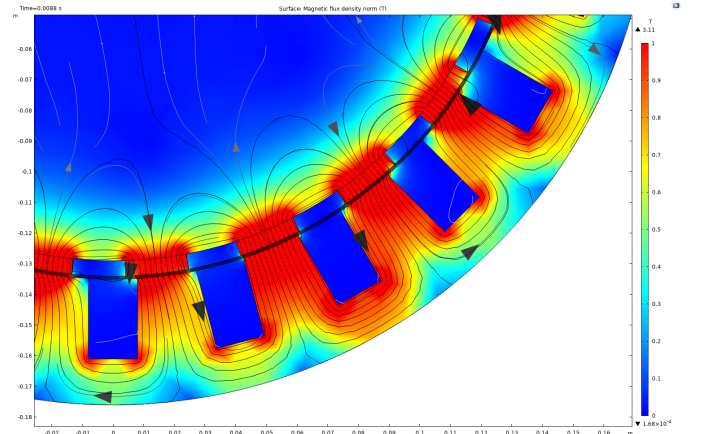


Fig. 33. Flux density plot

3) *Flux density*: The flux density plot in Figure 33 shows that the set boundary for max flux density of 1 T is adhered, with only a few minor deviations. As expected, however, the flux density is higher than 1 T in sharp corners of the stator teeth, but this is not likely to affect the motor's performance. On the other hand, saturation in the iron could have led to losses and reduced motor performance and might have disrupted the harmonics needed to test the prototype.

### B. Thermal test

When the concern about whether the PLA in the coil forms could withstand the expected heat generated in the motor was raised, it was decided to perform a thermal test of the coils and coil forms. According to ScienceDirect [23] the glass transition of PLA is around 55°-60° Celsius, meaning that the coil forms would likely start warping around 50°-55° Celsius.

1) *Test setup:* All the coils were inserted into the stator and connected in series. The test was done using a VARIAC to apply a voltage with a frequency of 50 Hz over the coils, with a multimeter in series to measure the current. The voltage was slowly increased until the current reached the rated level of 3 A. A FLIR thermal camera was used to measure the temperature increase in the coils over time. The starting temperature was measured to be 22.8° Celsius. The FLIR was pointed at one of the coils and used to take a snapshot, where each snapshot contained the temperature data and a timestamp. Figure 34 displays an example of a snapshot from the FLIR measurements.

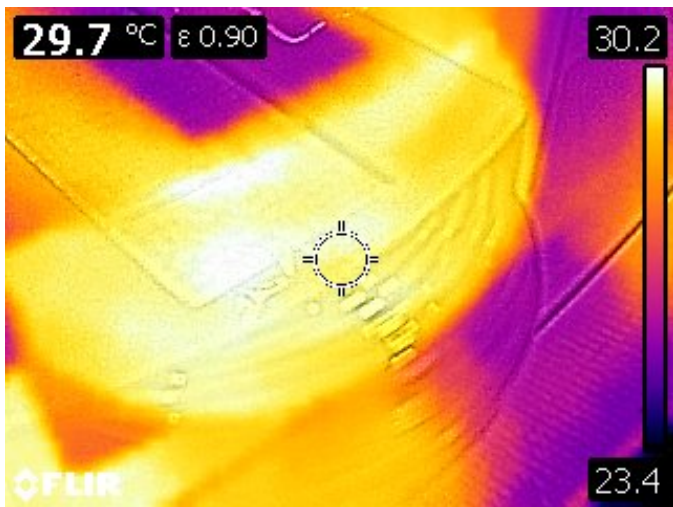


Fig. 34. Measurement from one coil during testing

2) *Results:* After 30 minutes, the temperature in the coils had started reaching an equilibrium at 38° Celsius. The snapshots from the FLIR were put into excel and plotted. A regression was done and plotted with the data points as seen in Figure 35, where the plots show the increase in temperature from room temperature. After 30 minutes, the motor was disconnected from the VARIAC. Once the motor had been disconnected, the coil forms were inspected to see if the PLA had become softer. It was concluded that at 38° Celsius, the rigidity of the forms was not noticeably different from room temperature.

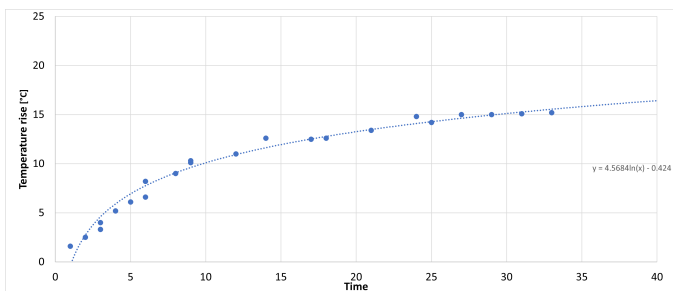


Fig. 35. Temperature rise test results and regression line

During the period when the motor was cooling down, the FLIR was used to measure the temperature during the cool down. A regression was also done for the cool-down period and plotted with the data points as seen in Figure 36, where the plot shows the decrease in temperature from 38° Celsius.

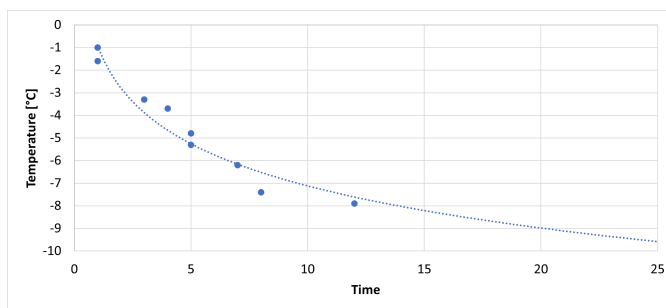


Fig. 36. Temperature decrease test results and regression line

### C. Back EMF-testing

After both the rotors were aligned in the prototype, a no-load test was performed on the prototype. Both rotors were rotated separately at various speeds. The back emf was measured using a FLUKE 434 series Power Quality Analyzer (PQA), while the rotational speed of the rotors was measured using a tachometer. The back emf test was not performed with both rotors rotating simultaneously due to the lack of drives to drive both rotors during the thesis period.

The data measured can be seen in Figure 37. Comparing the two curves for the phase voltages generated by the two rotors, it is clear that the 26-pole rotor generates a higher voltage per RPM than the 22-pole rotor. This difference is to be expected as the electrical frequency generated by the two is different. However, when the phase voltages are plotted related to the electrical frequency as in Figure 38 there is no apparent difference in the output from the two rotors.

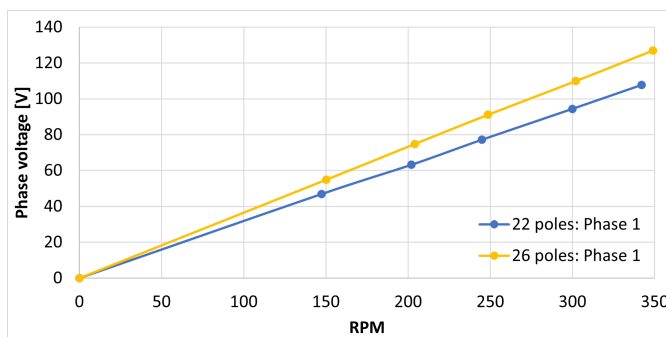


Fig. 37. Measured phase voltages related to measured RPM

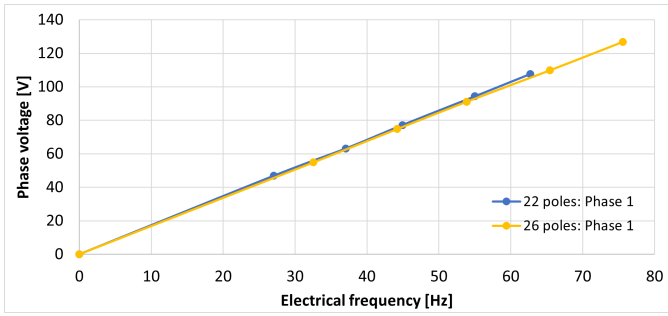


Fig. 38. Measured phase voltages related to measured frequency

Figure 39 shows the phase voltages per electrical frequency that were measured, plotted together with the data from COMSOL, and estimates from hand calculations using Equation 3.

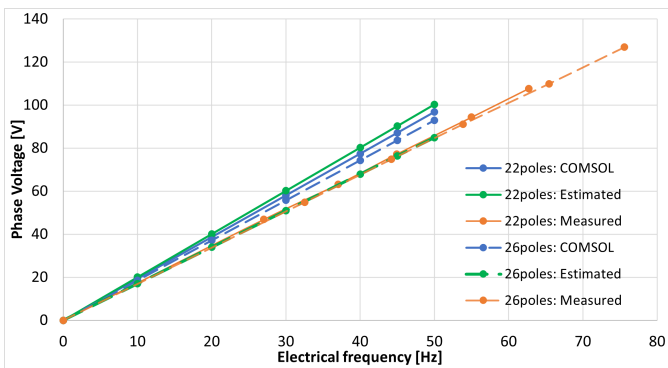


Fig. 39. Comparison between phase voltages measured in the tests, in COMSOL and hand calculations

Table VI and VII show that the phase voltages from COMSOL were about 11% higher than the actual results measured in the lab tests. Some of the reasons for this might be because the 2D COMSOL models only account for the length of 40 mm for the rotors and therefore neglect the iron losses from the extended stator that the prototype has in reality as well as the flux density might be lower in reality compared to simulations.

TABLE VI  
COMPARISON OF THE 22-POLE ROTOR

| COMSOL-Estimated | COMSOL-Measured | Estimated-Measured |
|------------------|-----------------|--------------------|
| -3.7 %           | 11.3 %          | 14.5 %             |

TABLE VII  
COMPARISON OF THE 26-POLE ROTOR

| COMSOL-Estimated | COMSOL-Measured | Estimated-Measured |
|------------------|-----------------|--------------------|
| 8.7 %            | 10.9 %          | 2.4 %              |

The measurements also showed that the phases were almost identical. During the 350 RPM measurements of the 26-pole rotor, the voltages were 126.9, 128.4 and 127.8 volts. The

largest difference between the coils were therefore only 1.2%, which is considered satisfactory.

Figure 40 shows the back emf from the two rotors. Comparing the curves for the two rotors, one can see that the voltage waveform is different, where the 26-pole rotor has a sharper peak voltage than the 22-pole rotor.

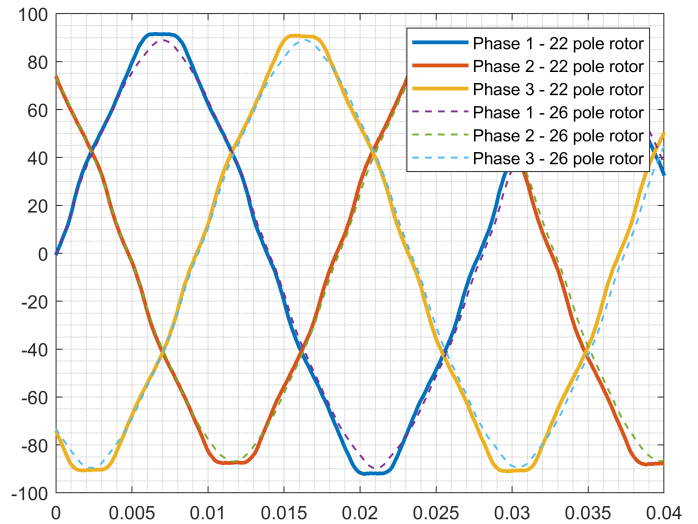


Fig. 40. Measured back emf for the two rotors

COMSOL models are simulated with one of the frequency measured and the back emf curves are compared with the measured ones in Figure 41. The measured voltage curves coincide very well with the simulated ones, where the simulated values only are slightly higher. This comparison indicates that the models are fairly accurate.

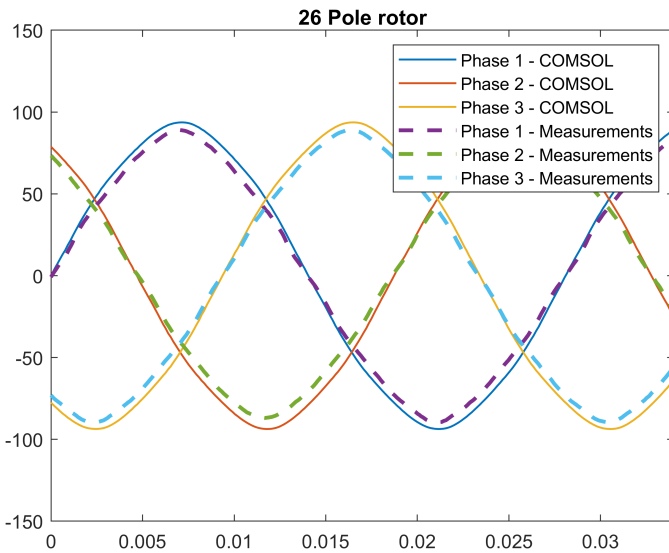
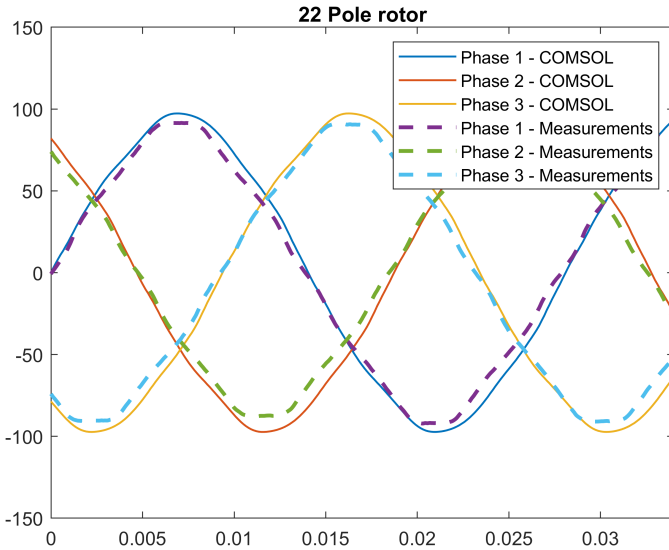


Fig. 41. Measured back emf compared to COMSOL values

#### D. Function test

A function test was performed on the prototype when both rotors were aligned. The function test was performed after the second rotor's first alignment and after the second rotor was upgraded with a larger shaft and center bearing. The function test was performed to prove that the twin harmonic motor drive concept was possible. In addition, the first function test was performed to check if the second rotor's cogging was too severe to perform any further tests.

1) *Setup:* The function test was performed by connecting a converter from Danfoss called VLT AutomationDrive FC 302 to the prototype. It is a three-phase converter functioning using linear voltage to frequency ratio that can be increased using a potentiometer as input. The converter must be connected to a 230 V IT system with an output voltage of 0 - 240 V and a power rating of 0.75 kW. This converter had some limitations towards powering the prototype as the voltage and

power rating were below what the motor was designed for. The test setup can be seen in Figure 42.

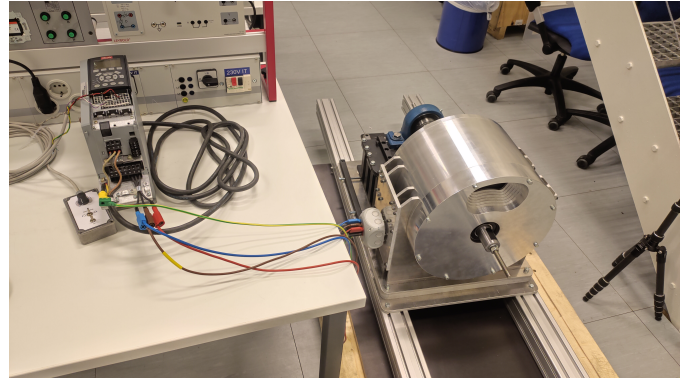


Fig. 42. Function test setup

2) *Result:* The first function test proved that the twin harmonic drive concept worked. However, during the first test, it was also discovered that the cogging on the second rotor was too severe for further tests. The cogging caused the motor to vibrate, and the speed was not increased beyond 48 RPM for the 22-pole rotor as the risk of damaging the prototype was too high. Therefore, the prototype had to be redesigned to align the 22-pole rotor better.

After the redesign and realignment of the second rotor, the function test was performed again. This time the cogging was unnoticeable, and the motor ran smoothly. However, while tuning the motor controller, some unexplainable behaviour was observed. When the controller surpassed 60 RPM referenced to the 26-pole rotor, the rotors seemed to stall and even rotate in directions opposite to what was expected. Future work will investigate this behaviour further.

## VI. DISCUSSION

As shown in the results from simulation and physical testing, driving two counter-rotating rotors by utilizing the twin harmonics in the stator is possible. The two rotors performed according to FAE simulations similarly regarding rotational speeds, torque output, cogging torque, back emf and phase voltages. Having two similar performing rotors was one of the first design criteria, where the gearing ratio was desired to be as close as possible. For larger machines with higher pole and slot numbers, the gearing could be even closer to one, and the rotors could have almost identical performances.

Looking at the back emf simulations, one can see that the shape of the voltage curve is different for the two rotors. This could indicate that the two rotors induce different harmonic content in the stator. The difference in voltage shape becomes clearer from the measured back emf, indicating that the harmonic content is larger in reality than in the COMSOL models. When comparing the simulated and the measured back emf, it is clear that the measurements coincide very well with the simulations regarding the voltage during separate

operations, where the simulated values only are about 10% higher. This comparison indicates that the models are fairly accurate; however, further testing is needed to verify the torque output. Sources of error and reasons for the differences between the FEA models and the measurements could be the material settings in the models, different magnetic properties set in the models or inaccurately wound coils.

The end-effect is one of the other effects of the design choices that did not come forth in the simulations. Because the stator is much longer than the rotors, the end-effects affecting the rotors might be noticeable. For example, the end-effects might lead to further cogging or disruption in the magnetic field. However, end-effects are believed mostly to lead to losses, which is irrelevant for testing this prototype. The stator length can be optimized after tests have been done on the prototype to define the optimal distance between the two rotors.

The reduction of turns that had to be done to fit the coils resulted in a lower voltage and higher current rating for the machine. The current rating for the motor was decided to be set to 3 A and not the 3.3 A the current had to be increased to for keeping the 2 kW power rating. This led to the new power rating of 1.8 kW. Reducing the power rating was not considered a problem as the prototype's main goal was to prove the concept of twin harmonic drive. As the coil wire is rated to handle the needed current, reaching the initially specified power rating is possible. The limitation factor for the power rating would most likely be the heat generated from the coils into the coil forms rather than the current rating of the wire. Using 3D printed coil forms eased both the winding process and the gluing of the coils to the stator. The coil forms also made the iterative process easier and could be considered ideal for prototyping. However, the coil forms did become the limiting factor for the temperature rating of the prototype, but as the performance of the prototype was not the objective of the motor, it ended up as a good decision. The thermal test that was done on the motor also proved that the coil forms would survive nominal operation continuously for 30 minutes, where the max temperature measured was 10° Celsius below the glass transition temperature of PLA. The motor was never intended to be operated with high performance over long periods, so the thermal test concluded that the PLA coil forms were good enough for this project. To increase the temperature rating, the printing filament used for the coil forms could have been changed from PLA to PTE-G, ABS or other heat-resistant filaments that can withstand temperatures up to 100° Celsius. The choice of using PLA filament was made because it would not lead to delays due to the need for ordering new filament. The coil forms also limited the machine's performance by reducing the useful slot area by about 50 mm<sup>2</sup>. Using a more traditional way of securing the coils than 3D printed coil forms, such as using wedges, is recommended for higher performance machines.

The motor was designed with one adjustable rotor so that the influence that the rotors have on each other can be tested using the prototype. The first iteration of the setup for the

adjustable rotor was a bad design as the magnetic forces pulling the rotor out of alignment were underestimated. After the cover with a center bearing was made for the adjustable rotor, the alignment process became much simpler. However, an adjustable rotor is not recommended for future designs of a counter-rotation motor. The manufacturing and alignment process of the adjustable rotor demanded much effort and time. For future designs, it is recommended to find an optimal distance between the two rotors and to have the two rotors stationary mounted, as this would reduce the complexity of the design and manufacturing drastically.

## VII. CONCLUSION

The main conclusion from the project is that the twin harmonic counter-rotation drive works as theorized. The concept of driving two counter-rotating rotors in one stator using magnetic field harmonics was proven during this project by designing, manufacturing and testing a prototype motor, where basic testing proved the concept. The COMSOL simulations that were done to confirm the counter-rotation were to some degree verified through no-load tests; however, further verification is needed. Back emf measured in the no-load test on the prototype deviated about 10% from the simulated values from COMSOL. The design topology of the prototype setup with two counter-rotating rotors made the manufacturing process especially difficult, as each shaft can only be supported on one side.

## VIII. FUTURE WORK

As the production of the motor took much more time than anticipated, much of the planned motor tests were not performed during the project period, and the prototype should therefore be tested more thoroughly. Nominal torque and cogging torque are parameters that should be validated from the COMSOL simulations through testing. Testing the influence the rotors have on each other through the planned rotor distance test is an important test that remains to be done on the prototype. Having one adjustable rotor proved to be a much larger inconvenience than expected, where the alignment of the adjustable rotor became very time consuming and labour-intensive. Therefore, testing the optimal rotor distance is important for the next dual rotor design. A working 3D model in COMSOL of the prototype should also be built and verified as this could be used to determine the optimal rotor distance for the next iteration of the twin harmonic counter-rotating motor.

Although the prototype worked as intended and proved that the drive of two counter-rotating rotors is possible using the twin harmonics, the design for a machine utilizing this should be optimized and analyzed further. The optimization of the motor was not done during this project since such a motor never had been built before and it was therefore hard to know what to optimize for. With the prototype built, extensive testing should be done to find the faults that can be optimized for the next iteration. The motor did behave strangely when the speed was increased over the electrical frequency of 13 Hz. What

the cause of this behaviour was, must be investigated further. This weird behaviour could be caused by the large amount of harmonic content fed by the 50 year old motor controller used for the function test or it could be caused by an other controller fault that is yet to be discovered. Because there have not been done much research on such a motor before, there is no established controller theory, and figuring out if the prototype can be controlled with standard motor controller theory remains to be investigated. The weird behaviour could also be caused by a fault in the design of the motor, where unexpected harmonic content is present at certain frequencies and as a result, space harmonics could be interacting with time harmonics. Therefore it is important to test the prototype further to optimize the control and design of the twin harmonic drive.

Whether utilizing the twin harmonics to drive two counter-rotating rotors is more efficient or better suited for any application than just putting two counter-rotating motors after each other is a question that this thesis did not look into and should therefore also be studied further. A comparison between the twin harmonic drive and two counter rotating motors in series should be done after the twin harmonic drive has been optimized.

#### IX. ACKNOWLEDGMENT

I want to thank Robert Nilssen for helping with his knowledge of the production of electric motors. Without his assistance, the design process would be much harder and more time-consuming. He also provided the Matlab script used to analyse the harmonics in the stator, which was essential for analysing if the counter-rotation was possible. In the ELK-22 course, Runar Møllerud gave instructions on how to make the COMSOL models that were used in this project which were very helpful. Dominik Häger has also come with essential input on what was needed in the CAD models for the prototype's production, which dimensions are common to use in different aspects of the motor. His expertise in mechanical production has been of great help throughout the project. Dominik was responsible for all the machining done on the prototype in-house at the NTNU. He came with the first draft of the prototype setup and the design for the second motor cover, the table for the adjustable rotor and the new shaft for the adjustable rotor. Finally, Michiel Desmedt must be mentioned. He has been a great help throughout the project, assisting with and being available for all my questions at any time of the day. He has helped with COMSOL simulations and furthered my understanding of magnetic gears and magnetic field harmonics. He has also been a major part of planning all the motor tests. A huge thanks to all of you!

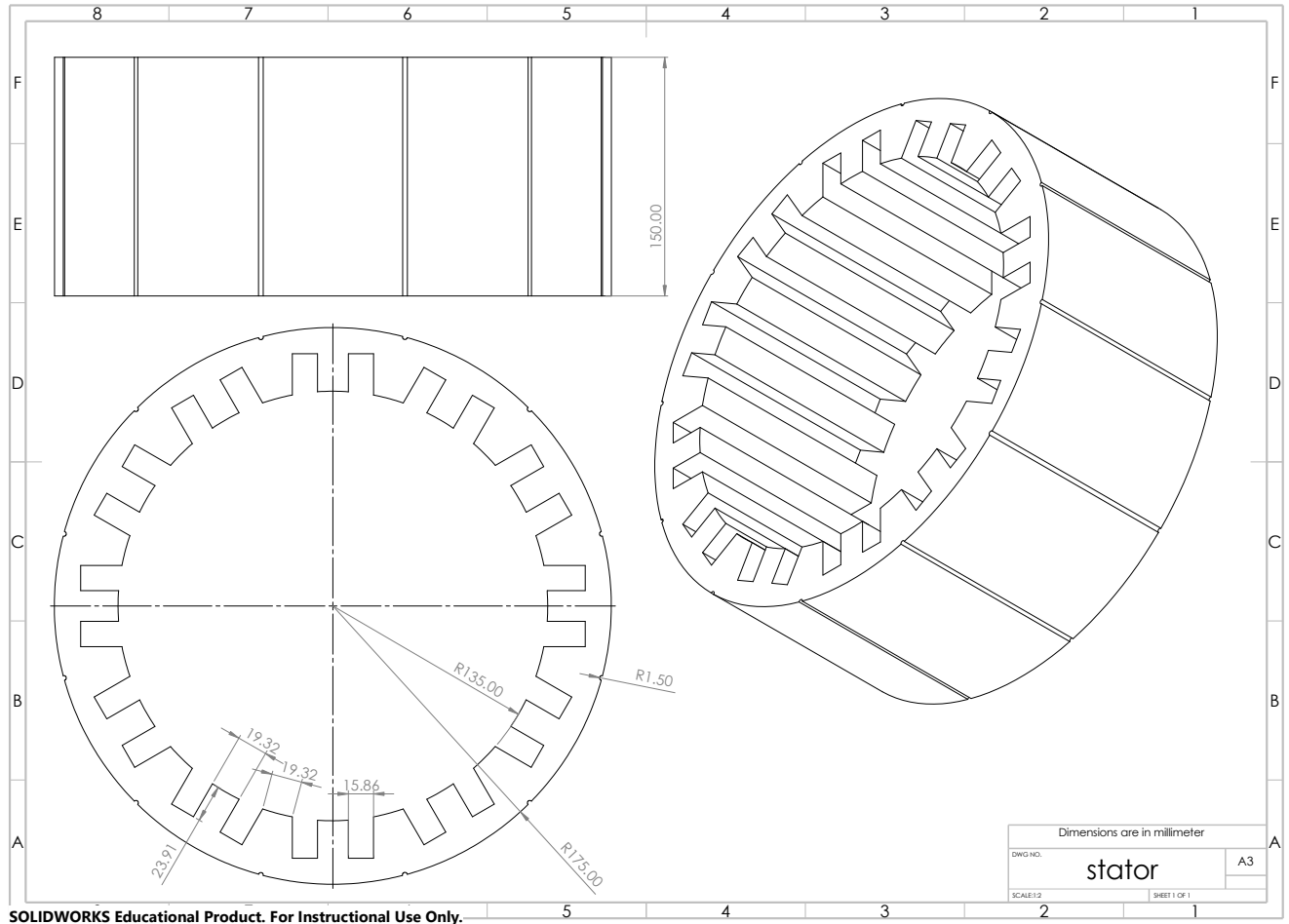
#### REFERENCES

- [1] S. Bergesen, "Design of a counter-rotating twin rotor machine prototype," Master's thesis, NTNU, 2021.
- [2] K. Vidyanandan and B. Kamath, "Grid integration of renewables: challenges and solutions," *Emerging Energy Scenario in India-Issues, Challenges and Way Forward*, 2018.
- [3] "Pumped storage hydropower." [Online]. Available: <https://www.hydropower.org/factsheets/pumped-storage>

- [4] "Kraftproduksjon." [Online]. Available: <https://www.nve.no/energi/energisystem/kraftproduksjon/>
- [5] P.-T. S. Storli, "Pumpeturbin i eksisterende kraftverk." [Online]. Available: <https://www.ntnu.no/hydrocen/2.3-pumpeturbin>
- [6] H. Hamnaberg and V. P. Consultant, "Pumpekraft i noreg," *Pumpekraft i Noreg- Kostnader og utsikter til potensial*, Oct 2011.
- [7] H. Dagsvik, "Pumpeturbiner i eksisterende kraftverk." [Online]. Available: <https://www.ntnu.no/hydrocen/pumpeturbiner-i-eksisterende-kraftverk>
- [8] J. Carlton, "Chapter 2 - propulsion systems," in *Marine Propellers and Propulsion (Third Edition)*, third edition ed., J. Carlton, Ed. Oxford: Butterworth-Heinemann, 2012, pp. 11–28. [Online]. Available: <https://www.sciencedirect.com/science/article/pii/B9780080971230000022>
- [9] O. E. H. Leangen, "Achieving counter-rotation by utilizing harmonic components of the magnetic field in a fractional slot concentrated winding permanent magnet motor," Master's thesis, NTNU, 2020.
- [10] D. P. Kothari, *Electric machines*, 5th ed. McGraw Hill Education (India), 2018.
- [11] S. Vaschetto, A. Tenconi, and G. Bramerdorfer, "Sizing procedure of surface mounted pm machines for fast analytical evaluations," *2017 IEEE International Electric Machines and Drives Conference (IEMDC)*, 2017.
- [12] G. P. S. Bimbhra, *Electrical Machines-I*. KHANNA PUBLISHING HOUSE. [Online]. Available: <https://books.google.no/books?id=LmIEEAAAQBAJ>
- [13] A. Zola, "What is harmonic?" Nov 2021. [Online]. Available: <https://whatis.techtarget.com/definition/harmonic>
- [14] F. Meier, "Permanent-magnet synchronous machines with non-overlapping concentrated windings for low-speed direct-drive applications," Ph.D. dissertation, KTH, 2008.
- [15] T. A. Lipo, *Introduction to AC machine design*. John Wiley & Sons, 2017.
- [16] J. Pyrhonen, T. Jokinen, and V. Hrabovcova, *Design of rotating electrical machines*. John Wiley & Sons, 2013.
- [17] Z. Zhu and D. Howe, "Influence of design parameters on cogging torque in permanent magnet machines," *IEEE Transactions on energy conversion*, vol. 15, no. 4, pp. 407–412, 2000.
- [18] P. Tlali, R. Wang, and S. Gerber, "Magnetic gear technologies: A review," in *2014 International Conference on Electrical Machines (ICEM)*. IEEE, 2014, pp. 544–550.
- [19] N. W. Frank and H. A. Toliyat, "Gearing ratios of a magnetic gear for marine applications," in *2009 IEEE Electric Ship Technologies Symposium*. IEEE, 2009, pp. 477–481.
- [20] W. AG, "Block magnet 40 x 20 x 5 mm, holds approx. 14 kg, nickel-plated." [Online]. Available: [https://www.supermagnete.de/eng/block-magnets-neodymium/block-magnet-40mm-20mm-5mm\\_Q-40-20-05-N](https://www.supermagnete.de/eng/block-magnets-neodymium/block-magnet-40mm-20mm-5mm_Q-40-20-05-N)
- [21] S. Meier, "Electric motor winding calculator." [Online]. Available: <https://www.emotor.com/windings/>
- [22] Yrkesopplæring and N. Standardiseringsforbund, *Verktstedshåndboka*, 6th ed. Yrkesopplæring ans, 2006.
- [23] "Poly (lactic acid)." [Online]. Available: <https://www.sciencedirect.com/topics/engineering/poly-lactic-acid>

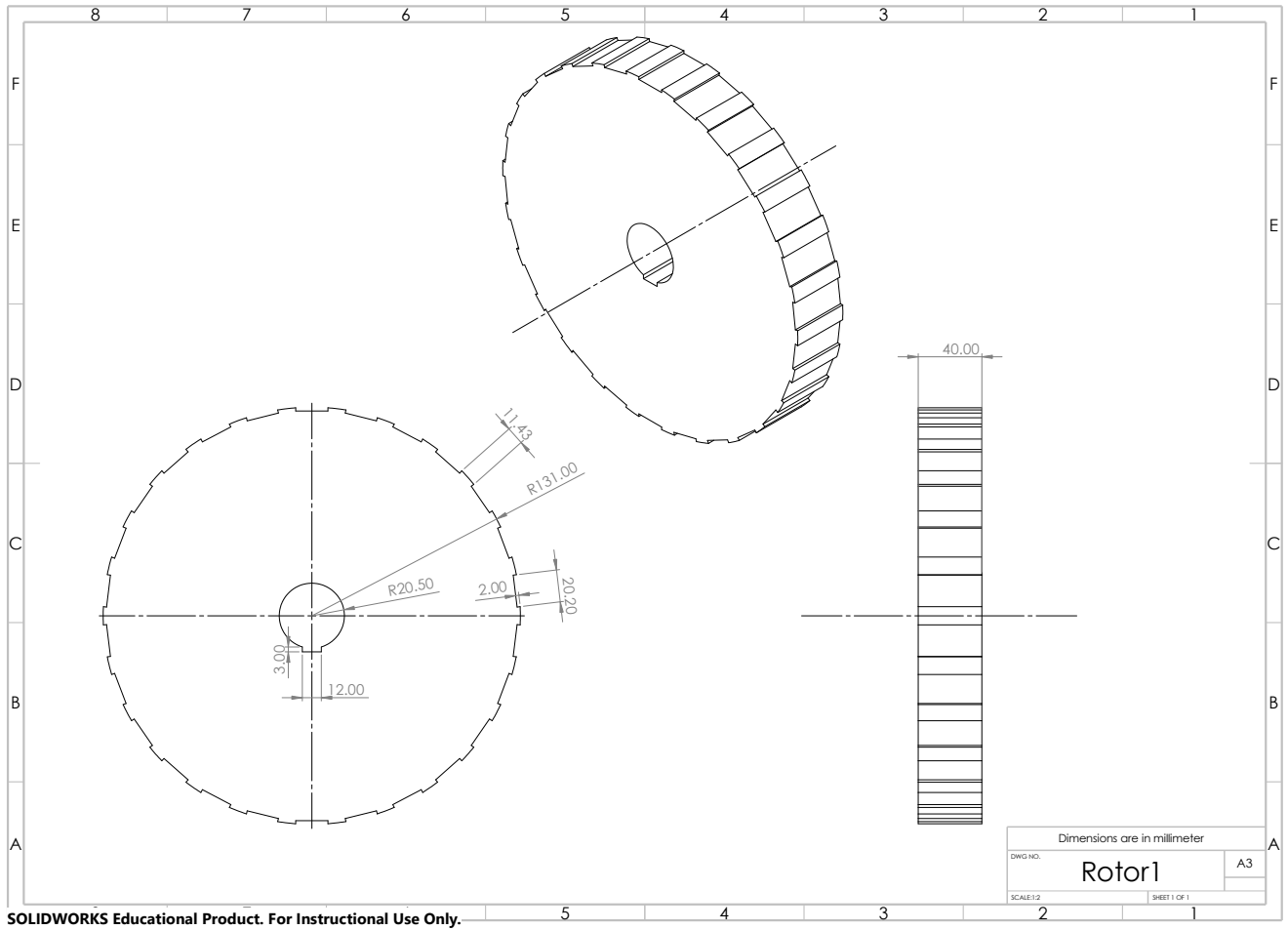
X. APPENDIX

A. Stator

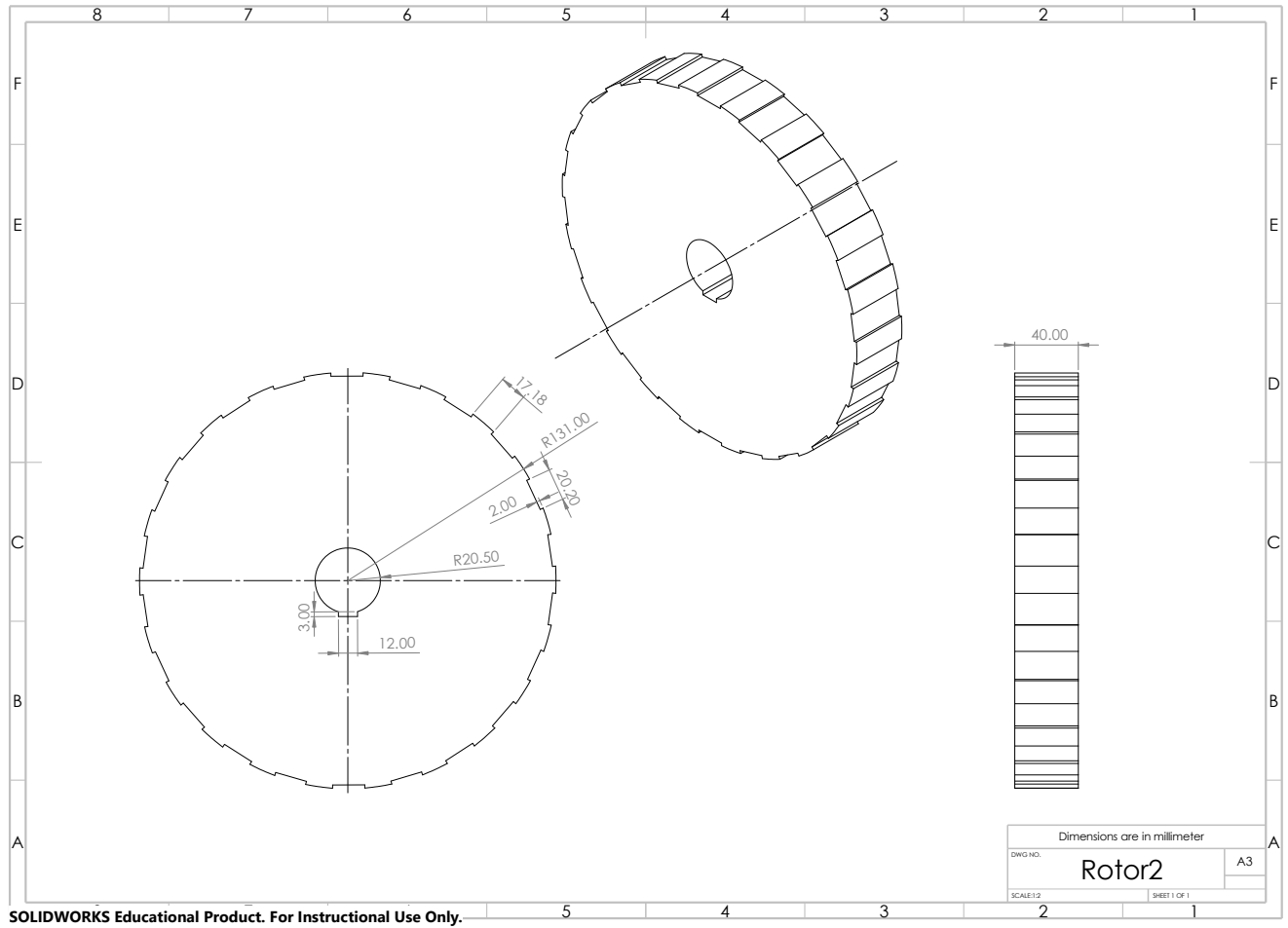


SOLIDWORKS Educational Product. For Instructional Use Only.

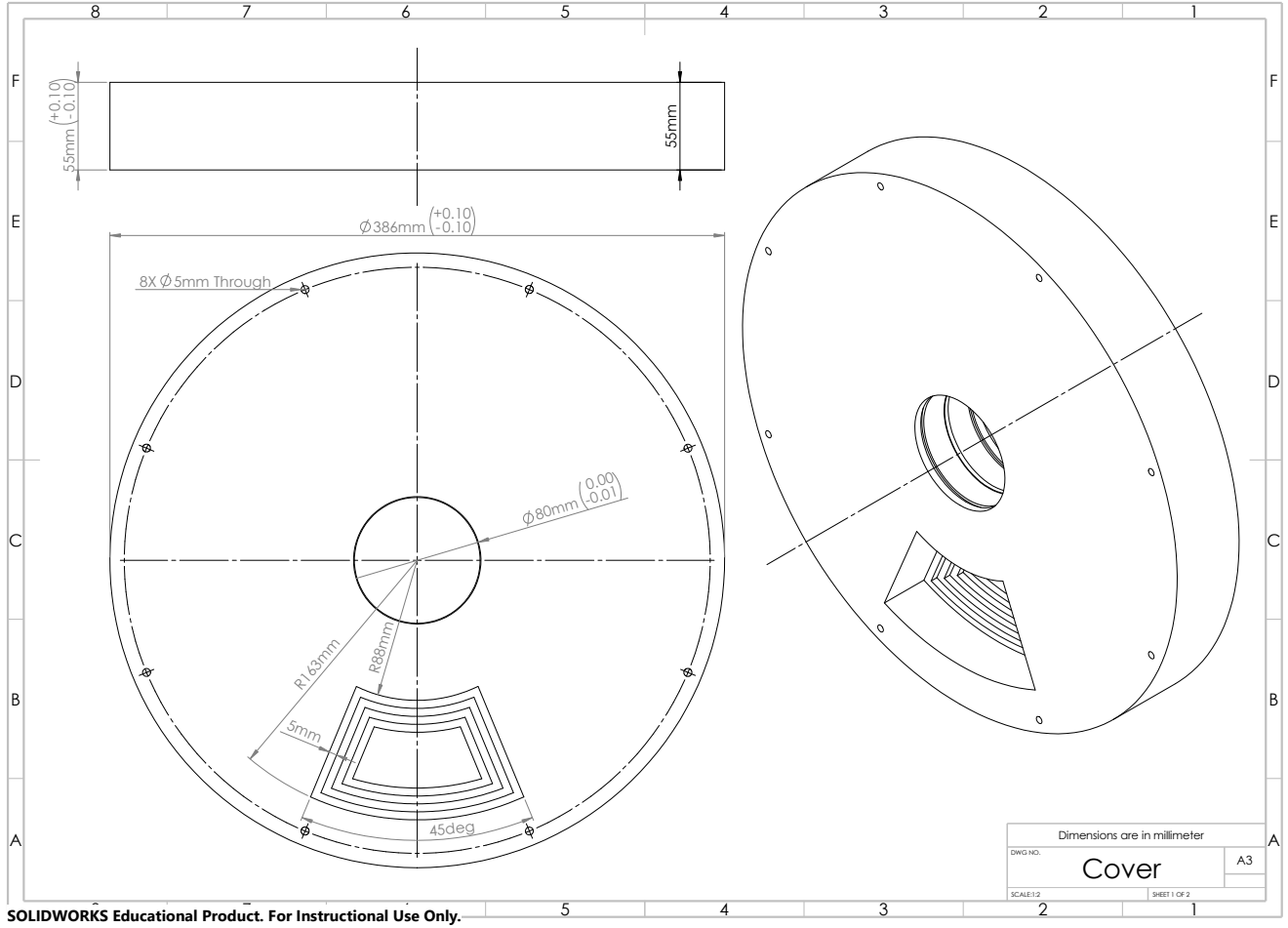
B. Rotor 26 poles

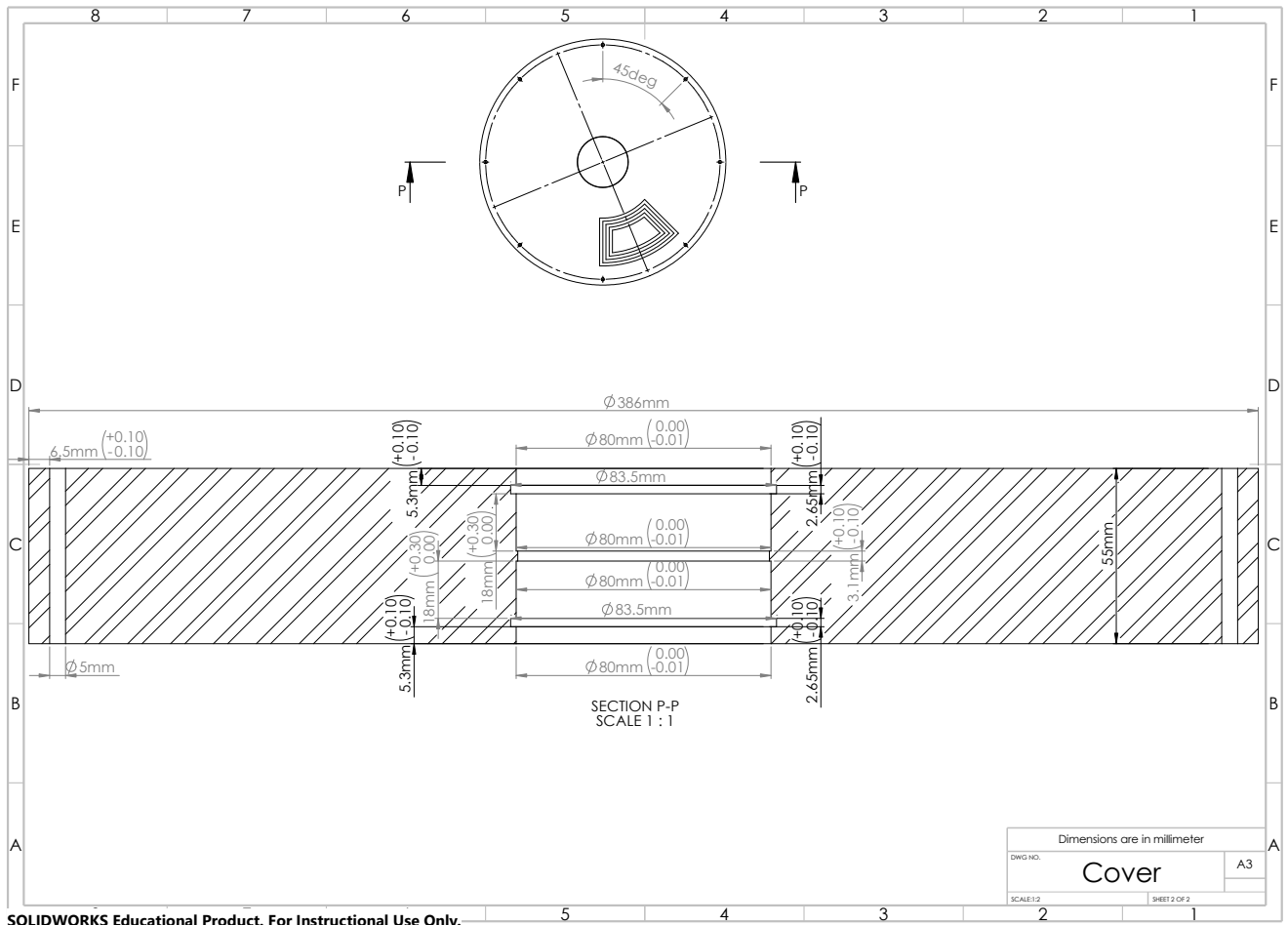


C. Rotor 22 poles



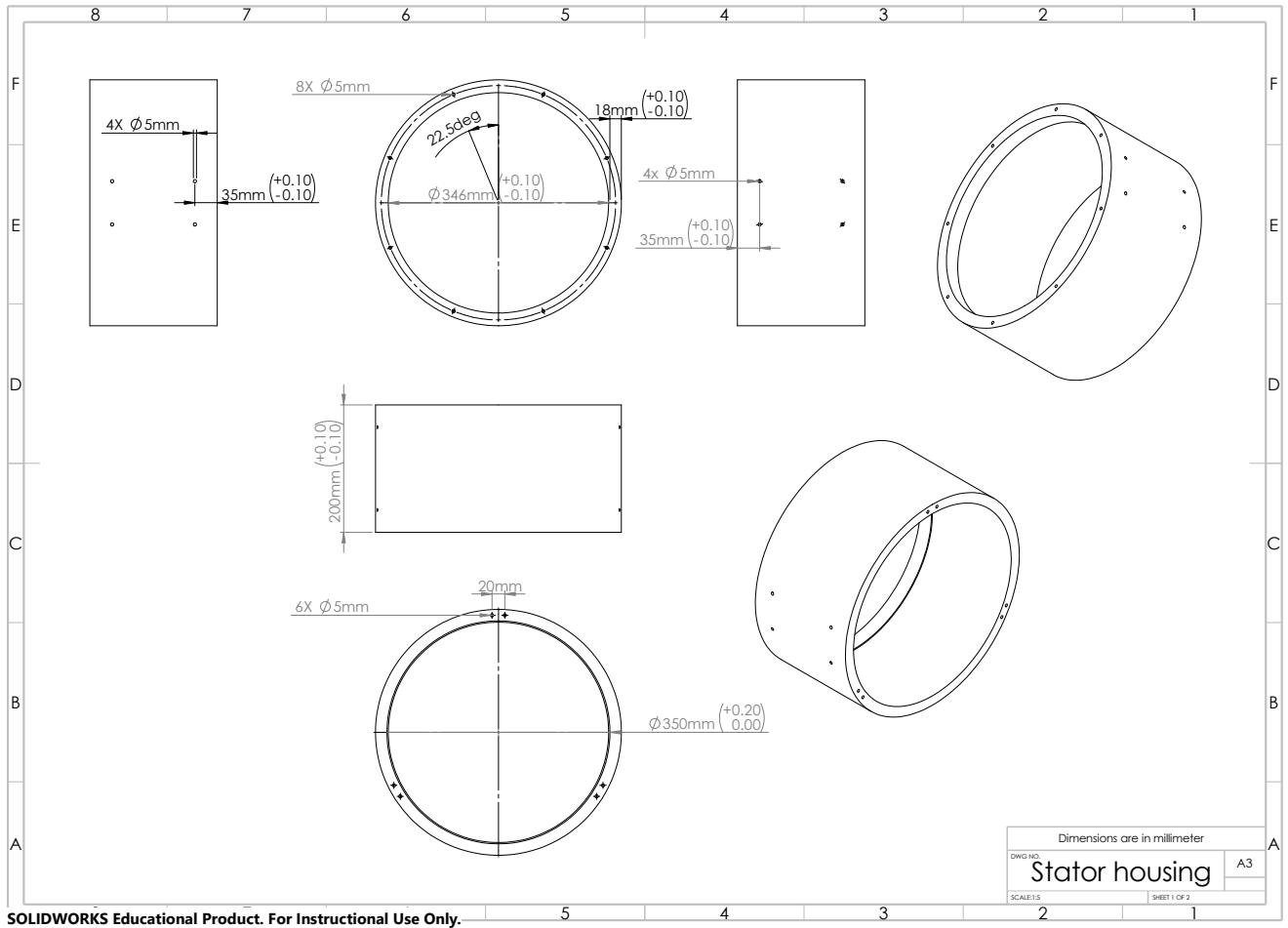
D. Cover

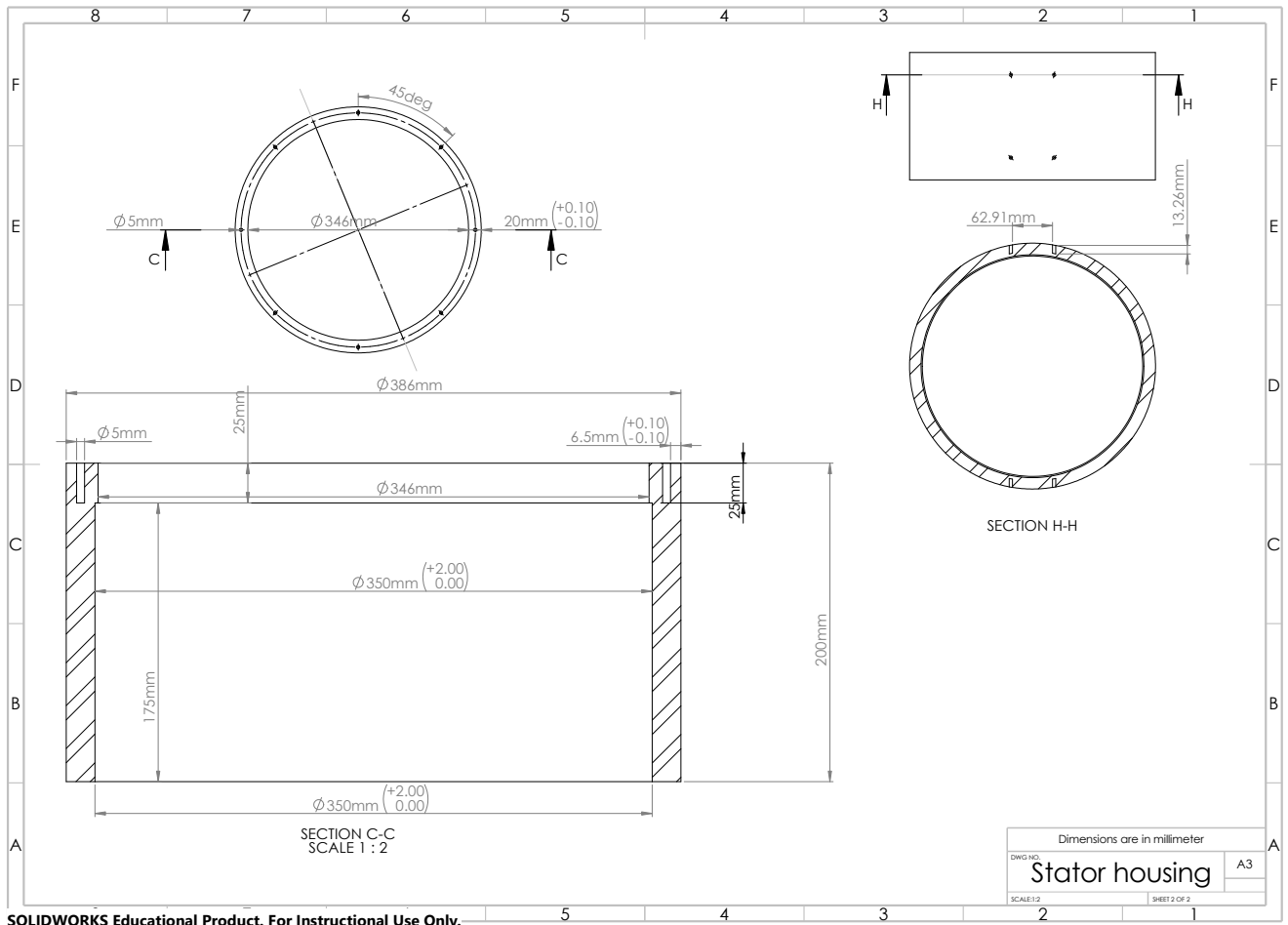




SOLIDWORKS Educational Product. For Instructional Use Only.

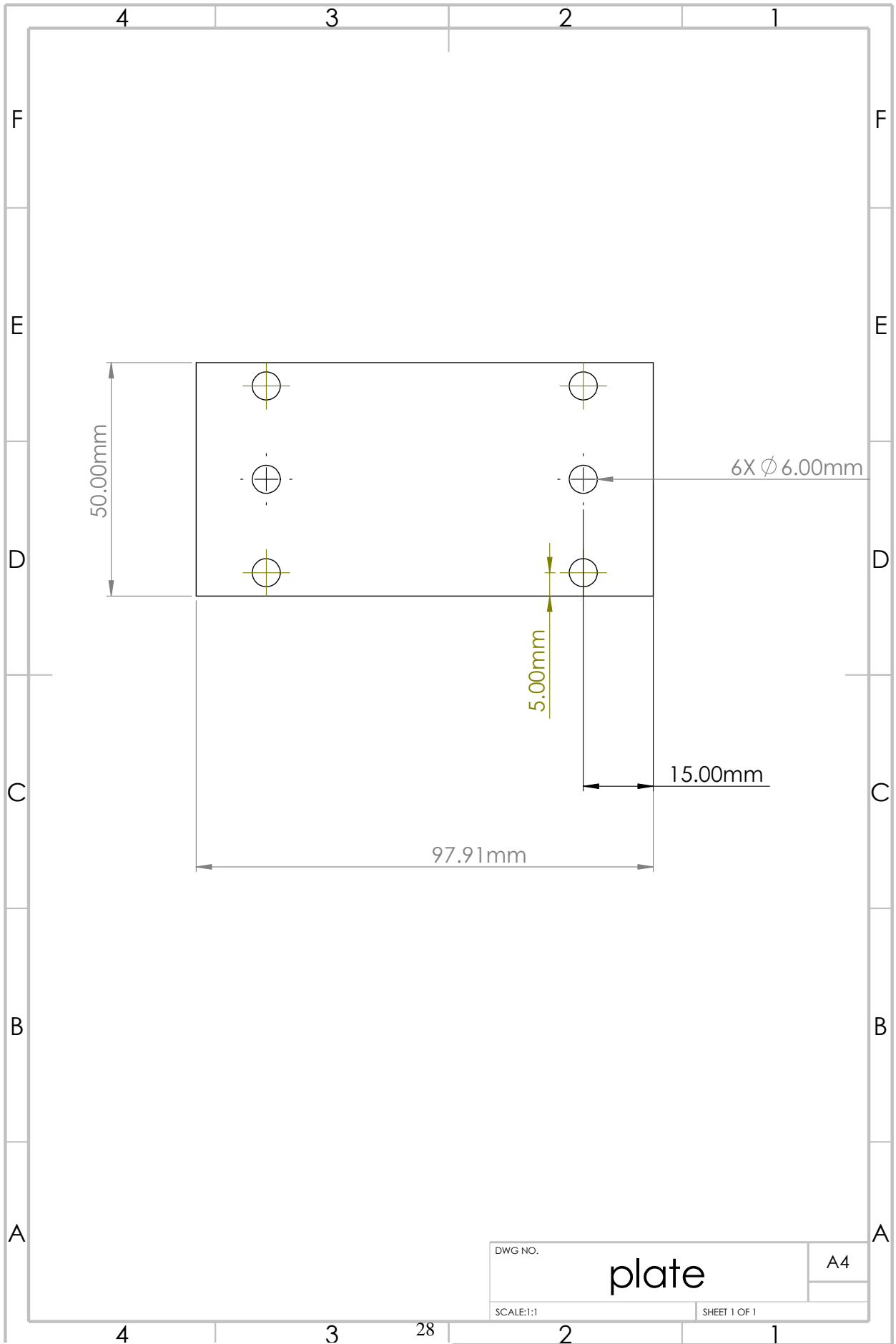
E. Stator housing

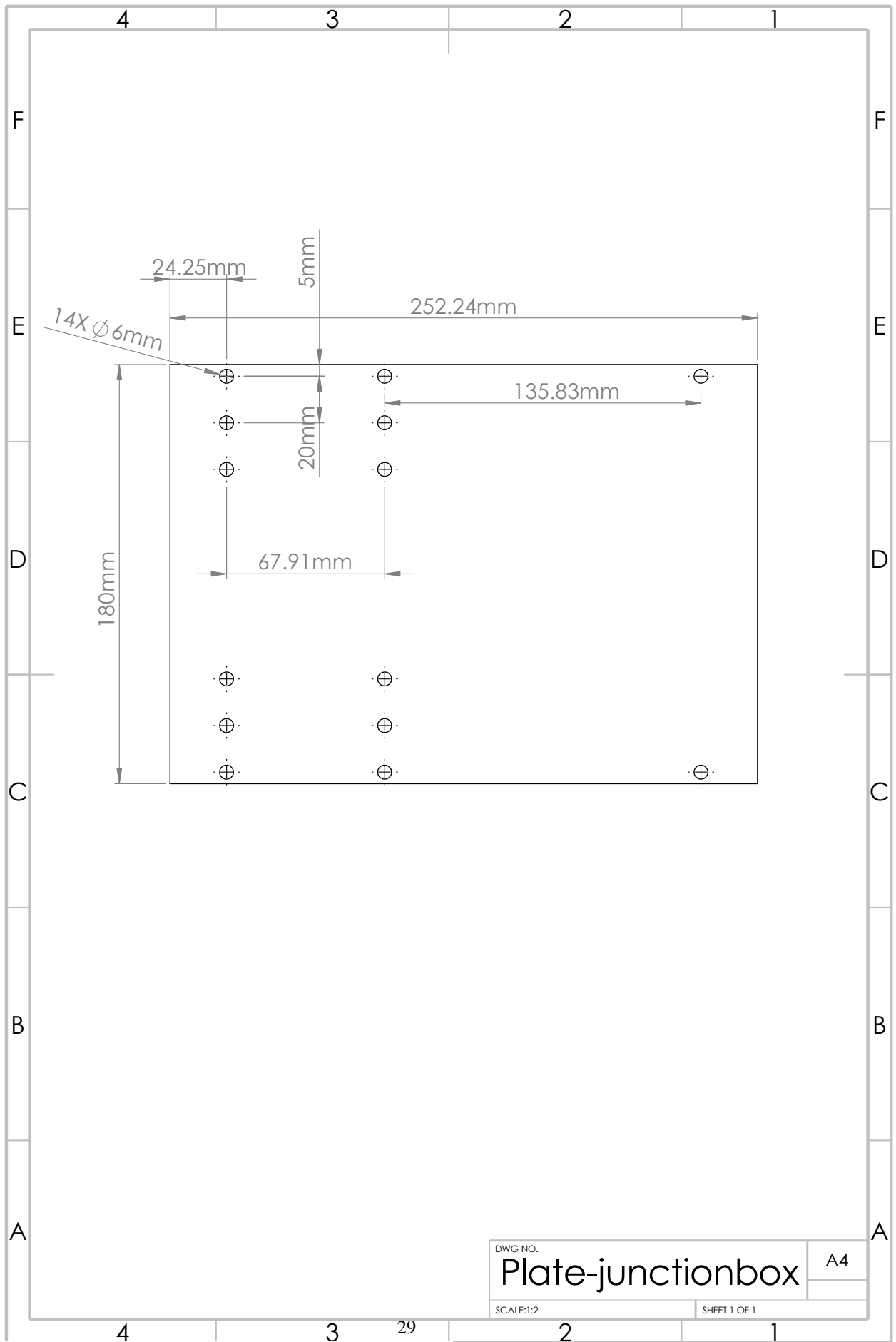


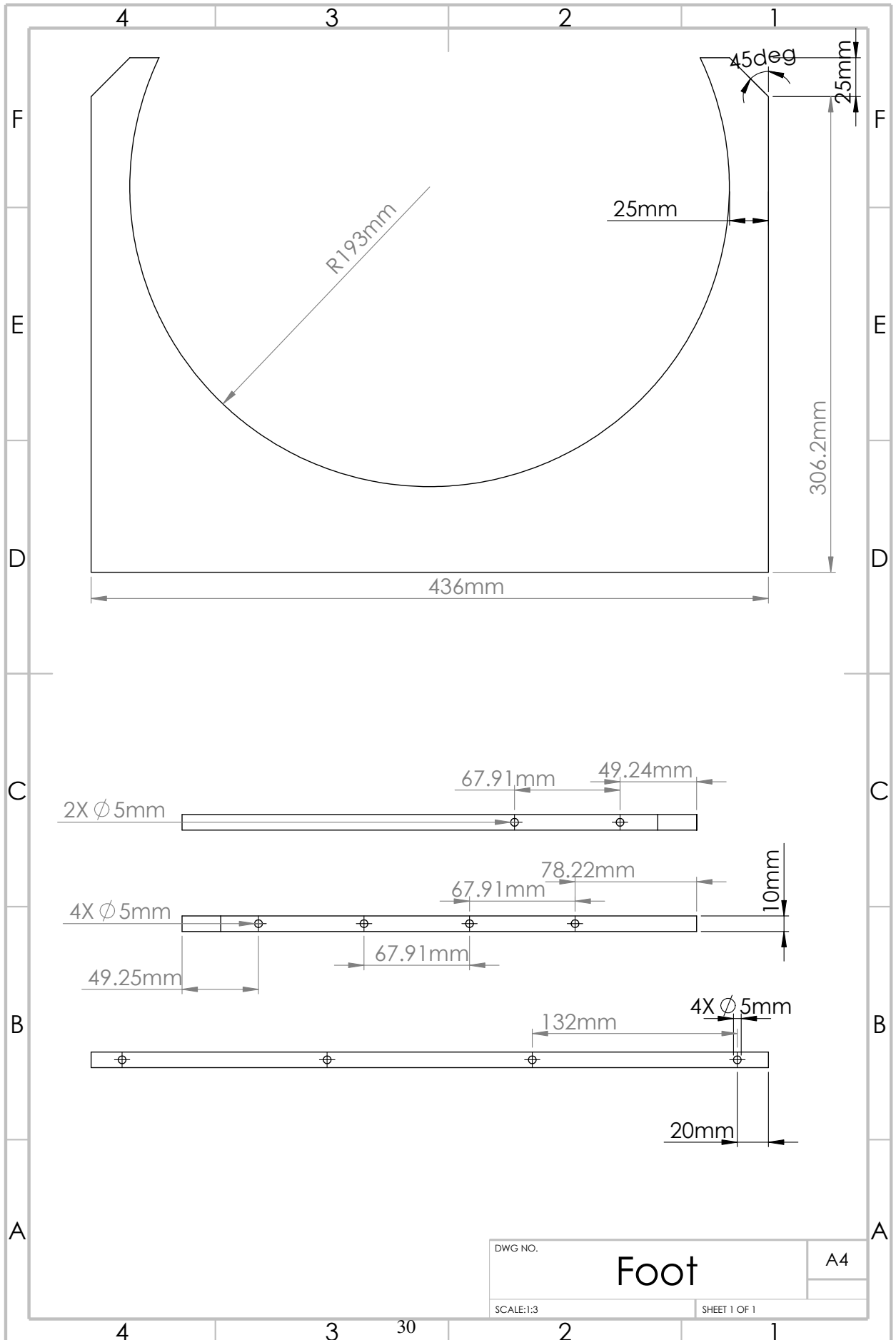


SOLIDWORKS Educational Product. For Instructional Use Only.

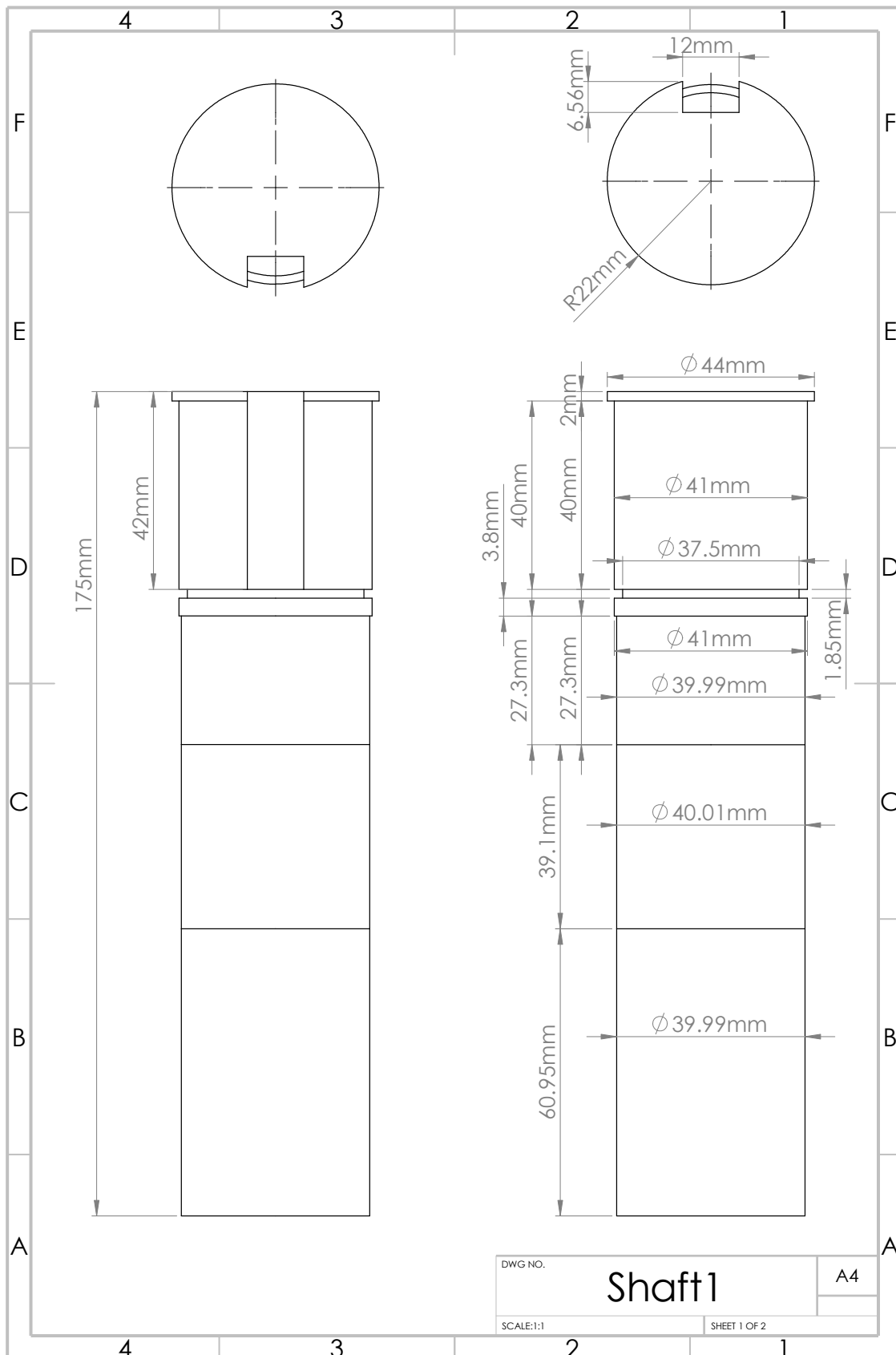








G. Shafts



|            |                 |              |
|------------|-----------------|--------------|
| DWG NO.    | <h1>Shaft1</h1> | A4           |
| SCALE: 1:1 |                 | SHEET 1 OF 2 |



